

# The impact of Lyman series photons on the intergalactic medium during the Epoch of Reionisation

Avery Meiksin

*SUPA\**, *Institute for Astronomy, University of Edinburgh, Blackford Hill, Edinburgh EH9 3HJ, UK*

3 November 2018

## ABSTRACT

The role of higher order Lyman series photons on the 21cm absorption or emission signature of the IGM against the background CMB during the Epoch of Reionisation is examined. It is shown that, taking into account the diminishing resonance line scattering cross section with increasing Lyman order, a non-negligible net scattering rate of higher order Lyman photons is expected. The resulting radiative cascades will substantially enhance the number density of Ly $\alpha$  photons near a radiation source. It is also shown that the higher order Lyman series photons are able to collisionally heat the IGM by amounts of tens to hundreds of degrees kelvin. The possibility that the Wouthuysen-Field effect may be suppressed by the presence of dust near a galaxy is discussed, and it is shown that the higher order Lyman series photons would still induce the effect, but with a somewhat reduced 21cm radiation efficiency. It is also demonstrated that extended low surface brightness emission line halos will be produced from radiative cascades following the scattering of higher order Lyman series photons. These halos would provide a unique means of confirming that reionisation source candidates were surrounded by an IGM that was still largely neutral on large scales.

**Key words:** atomic processes – cosmology: theory – line: formation – radiative transfer – radio lines: general – scattering

## 1 INTRODUCTION

The detection of the first sources of light in the Universe through their induced intergalactic H I 21cm signature before the Epoch of Reionisation (EoR) (Hogan & Rees 1979; Scott & Rees 1990; Madau et al. 1997) may be realised in the near to not very distant future with the advent of a new generation of metre-wavelength scale radio telescopes, such as the LOw Frequency Array (LOFAR)<sup>1</sup>, the Murchison Widefield Array (MWA)<sup>2</sup>, the Primeval Structure Telescope/21 Centimeter Array (PaST/21CMA)<sup>3</sup>, the Precision Array to Probe EoR (PAPER)<sup>4</sup>, and a possible Square Kilometre Array (SKA)<sup>5</sup>. Reviews of this rapidly growing area are provided by Fan et al. (2006) and Furlanetto et al. (2006). Central to the detection is the decoupling of the spin temperature of the neutral hydrogen from that of the Cosmic Microwave Background (CMB). Three possible decoupling mechanisms exist: coupling the energy levels to a

nearby bright radio source (Bahcall & Ekers 1969), establishing thermal equilibrium with the gas through collisions by other hydrogen atoms and electrons (Field 1958), and coupling the energy levels to Lyman resonance line radiation through the Wouthuysen-Field (W-F) effect (Wouthuysen 1952; Field 1958), which will normally quickly establish thermal equilibrium between the spin state and the scattering gas. At typical intergalactic densities at redshifts  $z < 17$ , where the signal may be detected by the newly developed or planned radio facilities, coupling through the scattering of Lyman resonance line photons is expected to be the dominant mechanism.

Whilst the discussion of the W-F mechanism has normally been confined to the context of hydrogen Ly $\alpha$  photons, the contribution of higher order Lyman resonance line photons has received recent attention (Barkana & Loeb 2005; Hirata 2006; Pritchard & Furlanetto 2006). Noting that the higher order photons will scatter only a few times before the excited atom decays through an alternative channel, it was concluded that direct collisions by higher order Lyman series photons would always be negligible compared with the Ly $\alpha$  collision rate of photons emitted directly by the source. At the same time, the Ly $\alpha$  photons produced in radiative cascades following the scattering of higher order Lyman series photons would provide a substantial boost to the overall

\* Scottish Universities Physics Alliance

<sup>1</sup> [www.lofar.org](http://www.lofar.org)

<sup>2</sup> [www.haystack.mit.edu/ast/arrays/mwa](http://www.haystack.mit.edu/ast/arrays/mwa)

<sup>3</sup> [web.phys.cmu.edu/~past](http://web.phys.cmu.edu/~past)

<sup>4</sup> [astro.berkeley.edu/~dbacker/eor](http://astro.berkeley.edu/~dbacker/eor)

<sup>5</sup> [www.skatelescope.org](http://www.skatelescope.org)

scattering rate. The amount of the boost would depend on the maximum upper principal quantum number  $n$  ( $n > 3$ )<sup>6</sup>, of the photons that are able to reach a given distance from the source without redshifting into the the resonance frequency of the next lower Lyman order.

In this paper, it is shown that the increasing mean free path through the IGM of higher order Lyman resonance line photons will result in a total scattering rate of Ly- $n$  photons a few percent of that of Ly $\alpha$  for sufficiently large upper principal quantum number  $n$ , much exceeding previous estimates. The enhancement of the Ly $\alpha$  scattering rate by Ly $\alpha$  photons produced in radiative cascades is found to boost the Ly $\alpha$  scattering rate by up to 30 per cent. more than previous estimates. It is also shown that since the higher order photons will not scatter sufficiently to establish thermal equilibrium with the gas, these photons may provide a non-negligible contribution to the heating of the IGM through collisional heating. The heating may be sufficient to raise the IGM temperature in the vicinity of a source above the CMB temperature, resulting in an emission signature against the CMB rather than absorption. Another consequence of the scattering of higher order Lyman series photons is the production of secondary emission lines, such as the Balmer and Paschen series, in radiative cascades in the neutral hydrogen surrounding the source. The emission lines would appear in the infra-red, and the emitting regions would subtend large angles on the sky, arising in spatially extended regions. Although the lines are individually weak, cross-correlations of the measurements of the expected lines may provide a detectable signal. The discovery of the emission line halos would provide a means of confirming that high redshift reionisation candidate sources were in fact embedded in an IGM that was still largely neutral on large scales.

Unless stated otherwise, a flat cosmology is assumed in this paper with a total mass density ratio to the Einstein-deSitter density of  $\Omega_m = 0.3$ , a vacuum energy contribution  $\Omega_v = 0.7$ , a baryon density  $\Omega_b h^2 = 0.02$ , and a Hubble constant of  $H_0 = 100h \text{ km s}^{-1} \text{ Mpc}^{-1}$  with  $h = 0.7$ .

## 2 THE SCATTERING OF INTERGALACTIC LYMAN RESONANCE LINE PHOTONS

The optical depth through a homogeneous and isotropic expanding IGM of a Ly- $n$  photon (with upper state principal quantum number  $n$ ) emitted by a source at redshift  $z_S$  and received at redshift  $z$  at frequency  $\nu > \nu_{lu}$ , where  $\nu_{lu}$  is the resonance line frequency, is

$$\tau_\nu = \sigma_n \int_z^{z_S} dz' \frac{dl_p}{dz'} n_l(z') \varphi_V \left( a_n, \nu \frac{1+z'}{1+z} \right), \quad (1)$$

where  $n_l(z')$  is the number density of scattering atoms in the lower level at epoch  $z'$ ,  $\sigma_n = (\pi e^2/m_e c) f_{lu} \simeq 0.02643 f_{lu} \text{ cm}^2 \text{ Hz}$  is the total resonance line cross section,  $f_{lu}$  is the upward oscillator strength,  $\varphi_V(a_n, \nu)$  is the Voigt line profile normalized to  $\int d\nu \varphi_V(a_n, \nu) = 1$ ,  $a_n$  is the ratio of the decay rate to the Doppler width  $\Delta\nu_D = \nu_{lu} b/c$ , where

$b = (2k_B T/m_H)^{1/2}$  is the Doppler parameter of the gas at temperature  $T$  and  $c$  is the speed of light, and  $l_p$  is the proper path length.<sup>7</sup> In the Lorentz wing, expressed as a function of the normalised frequency offset  $x = (\nu - \nu_{lu})/\Delta\nu_D$ , the dimensionless Voigt profile  $\phi_V(a_n, x) = (\Delta\nu_D)\varphi_V(a_n, \nu)$  is well-approximated by  $\phi_V(a_n, x) \simeq a_n/(\pi x^2)$ . The differential proper line element evolves according to  $dl_p/dz = c/[H(z)(1+z)] \simeq (c/H_0)\Omega_m^{-1/2}(1+z)^{-5/2}$  in a flat universe at redshifts for which  $\Omega_m(1+z)^3$  dominates the contribution from the vacuum energy, where  $H(z)$  is the Hubble parameter at redshift  $z$ . In the limit of scattering in the blue wing, the optical depth along the path of a photon emitted at frequency  $x_e$  from a source at redshift  $z_s$  and received at frequency  $x$  (provided it has not passed through any resonance line centre en route) is given at large separations by

$$\tau_x \simeq x_1 \left( \frac{1}{x} - \frac{1}{x_e} \right) \quad \text{where} \quad x_1 = \frac{\sigma_n a_n \lambda_{lu} n_l(z)}{\pi H(z)} \quad (2)$$

(Furlanetto & Pritchard 2006; Higgins & Meiksin 2009), where  $\lambda_{lu}$  is the wavelength of the resonance transition.

In terms of the atomic constants,  $x_1$  may be expressed as

$$x_1 = \frac{2}{\pi} \left( \frac{\pi e^2}{m_e c} \right)^2 \frac{g_l}{g_u} f_{lu}^2 \frac{n_l(z)}{H(z)b}, \quad (3)$$

where  $m_e$  and  $e$  are the mass and charge of the electron. For large  $n$  transitions,  $f_{lu} \simeq (2^8/3e^4)n^{-3} \simeq 1.56n^{-3}$ , so that  $x_1$  decreases rapidly with increasing order as  $x_1 \sim n^{-6}$ . The effective mean free path of the photon as defined through  $\tau_x = l_p/l_{\text{mfp}}$ , where  $l_p(z_S, z) = \int_z^{z_S} dz' dl_p/dz'$  is the proper distance travelled by the photon, is given by

$$l_{\text{mfp}} = \frac{\pi}{3} \left( \frac{\pi e^2}{m_e c} \right)^{-2} \frac{g_u}{g_l} f_{lu}^{-2} \frac{bc}{n_l(z)} \left[ \left( 1 - \frac{1+z}{1+z_S} \right)^{3/2} \right] x, \quad (4)$$

so that the resonance line photon mean free path increases like  $n^6$  for large  $n$ . For sufficiently large  $n$ , the mean free path will match the proper distance  $l_p$  for even small values of  $x \sim \mathcal{O}(1)$ . Thus, whilst the scattering of lower order Lyman resonance line photons occurs in the Lorentz wing, at sufficiently high orders the scattering will shift to the line core. The scattering of higher order photons, however, is confined increasingly to the vicinity of the source with increasing order. This is because, in an expanding IGM, higher order Ly- $n$  photons may redshift into the next lower order. The redshift  $z_n$  to which a Ly- $n$  photon may travel from a source at redshift  $z_S$  is given by  $1+z_n = (1+z_S)[1 - (n-1)^{-2}]/[1 - n^{-2}]$ .

The Lyman resonance order at which the transition to core scattering occurs may be estimated as follows. The Voigt line profile is well-approximated in the core by

<sup>7</sup> For low Lyman orders, the optical depth is complicated by the presence of deuterium, which will produce a Gunn-Peterson trough across the Ly- $n$  profiles for  $x < 81.5 \text{ km s}^{-1}/b$ . For a  $D/H$  ratio of  $2.8 \pm 0.2 \times 10^{-5}$  (O'Meara et al. 2006), the deuterium optical depths are  $\tau_\alpha \simeq 16.6 \pm 0.5$ ,  $\tau_\beta \simeq 2.6 \pm 0.1$  and  $\tau_\gamma \simeq 0.92 \pm 0.03$  at  $z = 8$ . The IGM becomes optically thin to deuterium Ly- $n$  photons for  $n > 3$  at  $z = 8$  ( $n > 5$  at  $z = 20$ ). Since the results discussed in this paper rely predominantly on higher orders, as the direct collisional rates of these lower order Ly- $n$  photons (above Ly $\alpha$ ) are already strongly suppressed, the effect of deuterium is not included.

<sup>6</sup> Ly $\beta$  photons cannot decay to Ly $\alpha$ , but will decay to H $\alpha$  followed by two-photon emission.

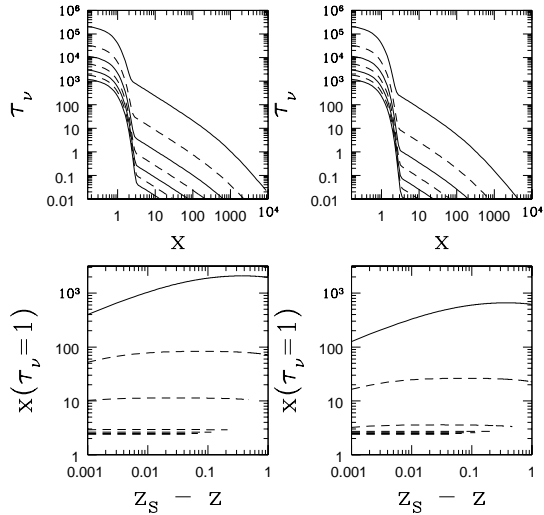


**Figure 1.** (Upper panels) The optical depth of photons emitted by a source at redshift  $z_S = 8$  and received at redshift  $z = 7.99$  at the frequency  $\nu$  near the resonance line frequency  $\nu_0$  for Ly $\alpha$  through Ly $\eta$  (top to bottom, alternating solid and dashed curves). The frequency is expressed as  $x = (\nu - \nu_0)/\Delta\nu_D$ , appropriate to each order. The left panel shows the optical depth for an IGM temperature of  $T = 10$  K and the right panel for  $T = 100$  K. (Lower panels) The values  $x_1$  of  $x$  at which  $\tau_\nu = 1$  for  $0.001 < z_S - z < z_S - z_n$  for a source at redshift  $z_S = 8$ , where  $z_n$  is the limiting redshift at which the frequency of an emitted Ly- $n$  photon redshifts into the next lower Lyman resonance frequency. The lines correspond, from top to bottom, to Ly $\alpha$  (solid line) through Ly $\eta$  (dashed lines for higher Lyman orders). The left panel shows the values of  $x_1$  for an IGM temperature of  $T = 10$  K and the right panel for  $T = 100$  K. (Not included is the effect of deuterium; see text.)

$\phi_V(x) \simeq \pi^{-1/2} \exp(-x^2)$ . For hydrogen gas in the temperature range  $10 < T < 1000$  K, the transition frequency  $x_m$  at which the core and wing approximations match lies in the range  $2.6 < x_m < 3.3$  for Lyman series photons with  $n < 8$ . A second order perturbation about  $x_m = 2.8$  gives the convenient approximation  $x_m \simeq 2.8(1 + \epsilon)$ , with  $\epsilon \simeq [0.5987 - 0.1131(5.208 + \log a)]^{1/2} - 0.7738$  (accurate to better than 0.1 per cent. for  $0.001 < a_n < 0.05$ ). It follows from Eq. (3) that Lyman resonance line photons with  $n \gtrsim 6$ , depending on the IGM temperature, will survive until redshifted into the resonance line core. In Figure 1, the intergalactic optical depths through an IGM at temperatures  $T = 10$  K and 100 K are shown for resonance line photons with  $n = 2 - 8$  emitted by a source at  $z_S = 8$ , along with the corresponding values of  $x_1$  as a function of redshift difference from the source. It is apparent that photons with  $n \geq 5$  or 6 will first scatter in the resonance line core.

The source function describing the injection of Lyman series photons following the initial scattering of continuum photons by the IGM is given by

$$S_n^{\text{inj}}(\nu) = n_l c \sigma_n \int_0^\infty d\nu' R_n(\nu', \nu) n_{\nu'}^{\text{inc}, n} \quad (5)$$

**Table 1.** Probabilities  $p_{n, n'}$  for a Ly- $n$  photon to convert into a Ly- $n'$  photon per scatter. The final column gives the survival probability  $p_{\text{surv}, n} = p_{n, n}$  for a Ly- $n$  photon to survive a scattering event as a Ly- $n$  photon.

$n$	$p_{n, n'=2}$	$p_{n, n'=3}$	$p_{n, n'=4}$	$p_{n, n'=5}$	$p_{\text{surv}, n}$
2	1.000000	0.000000	0.000000	0.000000	1.000000
3	0.000000	0.881665	0.000000	0.000000	0.881665
4	0.041993	0.000000	0.839041	0.000000	0.839041
5	0.056103	0.007435	0.000000	0.817749	0.817749
6	0.062869	0.011134	0.002231	0.000000	0.805282
7	0.066774	0.013232	0.003553	0.000885	0.797245
8	0.069291	0.014555	0.004380	0.001464	0.791712
9	0.071035	0.015452	0.004935	0.001850	0.787718
10	0.072306	0.016094	0.005327	0.002120	0.784728
11	0.073269	0.016573	0.005617	0.002318	0.782423
12	0.074020	0.016941	0.005838	0.002468	0.780605
13	0.074619	0.017231	0.006011	0.002584	0.779142
14	0.075107	0.017465	0.006149	0.002677	0.777946
15	0.075510	0.017657	0.006261	0.002751	0.776953
16	0.075847	0.017816	0.006354	0.002813	0.776120
17	0.076133	0.017950	0.006432	0.002865	0.775414
18	0.076378	0.018064	0.006499	0.002908	0.774808
19	0.076590	0.018162	0.006555	0.002945	0.774285
20	0.076774	0.018247	0.006604	0.002977	0.773830
21	0.076936	0.018321	0.006646	0.003005	0.773432
22	0.077078	0.018386	0.006684	0.003029	0.773080
23	0.077205	0.018443	0.006716	0.003050	0.772769
24	0.077317	0.018494	0.006746	0.003069	0.772491
25	0.077419	0.018540	0.006771	0.003086	0.772243
26	0.077510	0.018581	0.006795	0.003101	0.772020
27	0.077592	0.018617	0.006816	0.003115	0.771818
28	0.077666	0.018651	0.006834	0.003127	0.771635
29	0.077734	0.018681	0.006852	0.003138	0.771469
30	0.077796	0.018709	0.006867	0.003148	0.771318
31	0.077853	0.018734	0.006881	0.003157	0.771179

$$\simeq n_l \sigma_n \frac{L_{\nu_n}}{4\pi r_L^2 h_F \nu_n} \int_0^\infty d\nu' R_n(\nu', \nu) \exp(-\tau_{\nu'}),$$

(Higgins & Meiksin 2009), where  $n_{\nu}^{\text{inc}, n}$  is the specific number density of incident continuum photons near the resonance line frequency  $\nu_n$ . The incident photon number density near Ly- $n$  is given by  $n_{\nu}^{\text{inc}, n} = (4\pi/c)L_{\nu} \exp(-\tau_{\nu})/[(4\pi r_L)^2 h_F \nu]$  for a source of specific luminosity  $L_{\nu}$  and at a luminosity distance from the source  $r_L$ . It is clear that the source functions of Ly- $n$  photons depend on the order, particularly as a much smaller fraction of high order photons are scattered out of the line of sight from the source than low order. As a consequence, the scattering rate of higher order Lyman photons exceeds the rate of lower order Lyman photons (above Ly $\alpha$ ) for a nearly flat spectrum source.

The case of Ly $\alpha$  photons is special, since these photons cannot degrade. Instead, because the IGM is optically thick to Ly $\alpha$  photons the photons become trapped in the IGM until they redshift through the Ly $\alpha$  resonance as a consequence of cosmological expansion. A balance is then achieved between the injection rate and the escape rate of the photons from the IGM. The number of scatters  $\mathcal{N}_{\text{scat}}$  before the photons escape is given by the inverse of the Sobolev expansion parameter  $\gamma$ , which is the inverse of the Ly $\alpha$  optical depth in the expanding IGM,  $\mathcal{N}_{\text{scat}} = \gamma^{-1} =$

$\tau_\alpha = \lambda_\alpha \sigma_\alpha n_l(z)/H(z)$  (Field 1959a; Gunn & Peterson 1965; Madau et al. 1997).<sup>8</sup> The rate of photon scatters per hydrogen atom, given by integrating Eq. (5) over frequency, is then  $n_l^{-1} \int d\nu S_\alpha^{\text{inj}}(\nu) = n_\nu^{\text{inc},\alpha}(0) c \sigma_\alpha (a_\alpha/\pi) x_1^{-1}$ , approximating the Voigt profile by  $(a_\alpha/\pi) x^{-2}$ . Multiplying by the number of scatters  $\mathcal{N}_{\text{scat}}$  gives for the scattering rate per hydrogen atom,  $P_\alpha^{\text{direct}} = n_\nu^{\text{inc},\alpha}(0) c \sigma_\alpha$  since  $(a_\alpha/\pi)(\tau_\alpha/x_1) = 1$ . Thus the scattering rate is simply given by the scattering rate of the incident photons assuming no scattering losses en route (Field 1959a; Madau et al. 1997; Higgins & Meiksin 2009).

By contrast, Lyman resonance line photons above Ly $\alpha$  that first scatter in the wings will produce a negligible scattering rate because they will quickly degrade into a lower energy photon before they can redshift or diffuse into the resonance line core. A typical photon will not survive more than about five scatters (Pritchard & Furlanetto 2006). As will now be shown, higher order Lyman series photons that first scatter in the resonance line core will produce a non-negligible scattering rate, contrary to previous estimates which assumed a constant source function for all the Lyman resonance line photons (Barkana & Loeb 2005; Hirata 2006; Pritchard & Furlanetto 2006), leading to a scattering rate estimate of order  $\mathcal{O}(5 \times 10^{-6})$  times smaller than the Ly $\alpha$  rate.

The scattering rate per atom will depend on the total number density of resonance line photons built up in the region in which the incident radiation field generates them. For a mean scattering time of  $t_{\text{scat},n}(\nu) = 1/n_l c \sigma_n \phi_V(a_n, \nu)$  and a photon survival probability  $p_{\text{surv},n}$ , describing the fraction of Ly- $n$  photons that produce a subsequent Ly- $n$  photon upon scattering, the contribution of direct Ly- $n$  scatterings from the source to the photon number density, including the subsequent rescatterings of the photons, is given by

$$\begin{aligned}
n_\nu^{\text{direct},n} &= n_\nu^{\text{inc},n} \\
&+ n_l c \sigma_n p_{\text{surv},n} t_{\text{scat},n}(\nu) \\
&\times \int_0^\infty d\nu' R_n(\nu', \nu) n_{\nu'}^{\text{inc},n} \\
&+ \dots \\
&+ (n_l c \sigma_n p_{\text{surv},n})^{m+1} t_{\text{scat},n}(\nu) \\
&\times \int_0^\infty d\nu_m R_n(\nu_m, \nu) t_{\text{scat},n}(\nu_m) \dots \\
&\times \int_0^\infty d\nu_1 R_n(\nu_1, \nu_2) t_{\text{scat},n}(\nu_1) \\
&\times \int_0^\infty d\nu' R_n(\nu', \nu_1) n_{\nu'}^{\text{inc},n} \\
&+ \dots
\end{aligned} \tag{6}$$

Here,  $R_n(\nu', \nu)$  is the frequency redistribution function for the scattered photons. The survival probabilities  $p_{\text{surv},n}$  fol-

<sup>8</sup> The equivalence  $\mathcal{N}_{\text{scat}} = \gamma^{-1}$  also follows from the IGM scattering problem of Higgins & Meiksin (2009), who obtain an equilibrium photon number density  $n_\nu = \dot{s}/(n_l c \sigma_\alpha \gamma)$  in the red wing produced by the redshifting of photons following their injection by a Dirac  $\delta$ -function source of strength  $\dot{s}$  at a frequency  $\nu_{\text{inj}}$ , describing the trapping and rescattering of photons in the blue wing by the IGM. In equilibrium, the photons in the red wing must redshift away at the rate  $\int d\nu n_\nu / (\mathcal{N}_{\text{scat}} t_{\text{scat}}) = \dot{s}$ , giving  $\mathcal{N}_{\text{scat}} = \gamma^{-1}$ .

**Table 2.** The ratio  $\mathcal{N}_{\nu_n}/\mathcal{N}_{\nu_n}^{\text{inc}}(0)$  of Ly- $n$  photon occupation number to the occupation number from the incident radiation field assuming an optically thin IGM, divided by the IGM suppression factor  $\mathcal{S}_n$ , followed by the value of the suppression factor, for a source at redshift  $z_S = 8$  and a  $T = 10$  K IGM, at (proper) distances from the source of 20 kpc (cols 2–3) and 100 kpc (cols 5–6). For Ly $\alpha$ , only  $\mathcal{N}_\alpha/\mathcal{N}_\alpha^{\text{inc}}(0)$  is shown. Also provided are the corresponding light temperatures  $\langle T_n \rangle_{\text{H}}$  due to the direct radiation field  $n_\nu^{\text{direct},n}$  (cols 4 and 7).

$n$	$\frac{\mathcal{N}_{\nu_n}}{\mathcal{N}_{\nu_n}^{\text{inc}}(0)\mathcal{S}_n}$	$\mathcal{S}_n$	$\langle T_n \rangle_{\text{H}}$	$\frac{\mathcal{N}_{\nu_n}}{\mathcal{N}_{\nu_n}^{\text{inc}}(0)\mathcal{S}_n}$	$\mathcal{S}_n$	$\langle T_n \rangle_{\text{H}}$
2	8.88360	...	...	5.11169	...	...
3	17.4419	0.000022	-6.1130	14.7196	0.000015	-7.6446
4	9.77899	0.000042	-0.6605	8.02393	0.000037	-0.6873
5	7.14941	0.000075	-0.0737	6.20837	0.000071	-0.0739
6	5.89017	0.000137	-0.0483	5.42872	0.000135	-0.0483
7	5.32458	0.000225	-0.0440	5.06954	0.000224	-0.0440
8	5.02326	0.000342	-0.0436	4.87066	0.000342	-0.0436
9	4.84420	0.000494	-0.0442	4.74756	0.000494	-0.0442
10	4.72910	0.000684	-0.0451	4.66522	0.000683	-0.0451
11	4.65052	0.000916	-0.0462	4.60691	0.000916	-0.0462
12	4.59430	0.001195	-0.0473	4.56379	0.001195	-0.0473
13	4.55252	0.001525	-0.0483	4.53078	0.001526	-0.0483
14	4.52051	0.001910	-0.0494	4.50481	0.001911	-0.0494
15	4.49536	0.002356	-0.0505	4.48394	0.002356	-0.0505
16	4.47516	0.002864	-0.0516	4.46684	0.002866	-0.0516
17	4.45866	0.003441	-0.0526	4.45263	0.003443	-0.0526
18	4.44495	0.004091	-0.0537	4.44066	0.004092	-0.0537
19	4.43343	0.004817	-0.0548			
20	4.42363	0.005624	-0.0558			
21	4.41521	0.006516	-0.0569			
22	4.40791	0.007497	-0.0579			
23	4.40153	0.008572	-0.0590			
24	4.39592	0.009745	-0.0601			
25	4.39095	0.011020	-0.0612			
26	4.38652	0.012402	-0.0623			
27	4.38256	0.013894	-0.0634			
28	4.37900	0.015501	-0.0645			
29	4.37579	0.017227	-0.0657			
30	4.37288	0.019077	-0.0668			
31	4.37024	0.021055	-0.0680			

low from the spontaneous transition rates  $A(n, l; n', l')$  according to

$$p_{\text{surv},n} = A_{n,1}^{-1} A(n, 1; 1, 0), \tag{7}$$

where  $A_{n,l} = \sum_{j=1}^{n-1} \sum_{k=0}^{j-1} A(n, l; j, k)$  denotes the total decay rate from level  $(n, l)$  to all lower levels. Values for  $n = 2$  to 31 are provided in Table 1.

The direct Ly- $n$  scattering rate is given by integrating  $n_\nu^{\text{direct},n}$  over the Ly- $n$  cross section. Noting that  $\int d\nu R_n(\nu', \nu) = \varphi_V(a_n, \nu')$ , the integrals in Eq. (6) contract, resulting in the direct scattering rate

$$\begin{aligned}
P_n^{\text{direct}} &= \int_0^\infty d\nu n_\nu c \sigma_n \varphi_V(a_n, \nu) \\
&= P_n^{\text{inc}} / (1 - p_{\text{surv},n}), \\
&= P_n^{\text{inc}}(0) \mathcal{S}_n / (1 - p_{\text{surv},n}),
\end{aligned} \tag{8}$$

where  $P_n^{\text{inc}}(0) = n_\nu^{\text{inc},n}(0) c \sigma_n = \sigma_n L_{\nu_n} / (4\pi r_L^2 h_P \nu_n)$  is the scattering rate for an optically thin IGM, and

$$S_n = \int_0^\infty d\nu' \varphi_V(a_n, \nu') \exp(-\tau_{\nu'}) \quad (9)$$

describes the scattering suppression factor due to the scattering out of source photons by the intervening IGM out to the distance  $r_L$  (Dijkstra et al. 2008; Higgins & Meiksin 2009). Values of  $S_n$  are tabulated in Table 2 for some typical situations.

Although the expression in Eq. (8) follows from a seemingly straightforward account of photon scatters, the expression for  $n_\nu^{\text{direct},n}$  in Eq. (6) reveals that an implicit non-trivial assumption has been made: it has been assumed that the photons rescattered from frequency  $\nu_j$  to  $\nu_{j+1}$  have sufficient time to do so before their frequencies are Doppler shifted relative to the expanding (or contracting) gas). Since the photons are initially scattered blueward of the line centre, redshifting will generally carry the photons to frequencies with larger scattering optical depths. If the redshifting timescale (characterised by the inverse of the divergence of the velocity field), is shorter than the scattering time at the frequency  $\nu_j$ , the redshifting timescale should be used in Eq. (6). In the case of a contracting region, blueshifting may carry the photons to regions of a longer mean free path, and hence longer scattering time. If the scattering time exceeds the contraction timescale, then scattering may not occur at all before the photons are blueshifted away, and so the contraction timescale should be used. These factors are further complicated by the redistribution of the photon frequencies by the scattering, which tends to drive photons towards the line centre for scatters not too far out in the wing, and to concentrate the photon frequencies at the incoming frequency for scatters well into the wings (eg, Mihalas (1978)). In the event the scattering time is shorter than the characteristic expansion or contraction timescale, Eq. (6) may be used, from which Eq.(8) follows.

Incident resonance line Ly- $n$  photons that do not rescatter as Ly- $n$  photons will produce lower order Lyman series photons through the ensuing radiative cascades, adding to the direct scattering rate above. The cascade rates may be estimated similarly to the above, except that the redistribution function must now describe the conversion of a Ly- $n$  photon to Ly- $n'$  ( $n' < n$ ). The Lyman photon conversion probabilities per scatter  $p_{n,n'}$  may be computed from the probability for an atom in state  $(n, l)$  to produce a Ly- $n'$  photon through radiative cascades,

$$p_{\text{casc}}(n, l; n') = A_{n,l}^{-1} \sum_{j=n'}^{n-1} \sum_{k=0}^{j-1} A(n, l; j, k) p_{\text{casc}}(j, k; n'). \quad (10)$$

The values for  $p_{\text{casc}}(j, k; n')$  may be computed iteratively from low  $j$  to high, initiated by  $p_{\text{casc}}(n', 1; n') = p_{\text{surv},n'}$  and  $p_{\text{casc}}(n', k; n') = 0$  for  $k \neq 1$ . The Lyman photon conversion probabilities are then given by  $p_{n,n'} = p_{\text{casc}}(n, 1; n')$ . Values for  $n = 2$  to 31 and  $n' \leq 5$  are provided in Table 1.

The photon density  $n_\nu^{\text{direct},n}$  serves to source lower order photons through scatterings in which the original Ly- $n$  photon degrades into lower energy photons. Since every order will produce further lower order Lyman photons through scatterings, a production cascade of Lyman photons results. The rates may be computed by starting with the highest order Lyman resonance line photons,  $n_{\text{max}}$ , reaching a given distance from the central source. The production rate of the

next lower allowed Lyman order photons is

$$S_{n_{\text{max}}, n_{\text{max}}-2}(\nu) = n_l \sigma_{n_{\text{max}}} p_{n_{\text{max}}, n_{\text{max}}-2} \times \int_0^\infty d\nu' R_{n_{\text{max}}, n_{\text{max}}-2}(\nu', \nu) n_{\nu'}^{\text{direct}, n_{\text{max}}}, \quad (11)$$

where  $R_{n',n}(\nu', \nu)$  is the redistribution function describing the scattering of a Ly- $n'$  photon at frequency  $\nu'$  to a Ly- $n$  photon at frequency  $\nu$ . The redistribution function is discussed in the Appendix. The resulting density of cascade-produced  $n_{\text{max}}-2(\nu)$  photons, including their rescatterings, is then given by

$$\begin{aligned} n_\nu^{\text{cascade}, n_{\text{max}}-2} &= n_l c \sigma_{n_{\text{max}}} p_{n_{\text{max}}, n_{\text{max}}-2} t_{\text{scat}, n_{\text{max}}-2}(\nu) \\ &\times \left[ \int_0^\infty d\nu' R_{n_{\text{max}}, n_{\text{max}}-2}(\nu', \nu) n_{\nu'}^{\text{direct}, n_{\text{max}}} \right. \\ &+ n_l c \sigma_{n_{\text{max}}-2} p_{\text{surv}, n_{\text{max}}-2} \\ &\times \int_0^\infty d\nu_1 R_{n_{\text{max}}-2}(\nu_1, \nu) t_{\text{scat}, n_{\text{max}}-2}(\nu_1) \\ &\times \int_0^\infty d\nu' R_{n_{\text{max}}, n_{\text{max}}-2}(\nu', \nu_1) n_{\nu'}^{\text{direct}, n_{\text{max}}} \\ &+ \dots \\ &+ (n_l c \sigma_{n_{\text{max}}-2} p_{\text{surv}, n_{\text{max}}-2})^m \\ &\times \int_0^\infty d\nu_m R_{n_{\text{max}}-2}(\nu_m, \nu) t_{\text{scat}, n_{\text{max}}-2}(\nu_m) \dots \\ &\times \int_0^\infty d\nu_1 R_{n_{\text{max}}-2}(\nu_1, \nu_2) t_{\text{scat}, n_{\text{max}}-2}(\nu_1) \\ &\times \int_0^\infty d\nu' R_{n_{\text{max}}, n_{\text{max}}-2}(\nu', \nu_1) n_{\nu'}^{\text{direct}, n_{\text{max}}} \\ &\left. + \dots \right]. \quad (12) \end{aligned}$$

As in the case of  $n_\nu^{\text{direct},n}$  in Eq. (6), it has been implicitly assumed that the photons are not much redshifted (or blueshifted) relative to the scattering medium if it is expanding (or contracting) before being scattered. If not, then integrating  $n_\nu^{\text{cascade}, n_{\text{max}}-2}$  over the scattering cross-section contracts Eq. (12) into

$$P_{n_{\text{max}}, n_{\text{max}}-2}^{\text{direct-cascade}} = \frac{p_{n_{\text{max}}, n_{\text{max}}-2}}{1 - p_{\text{surv}, n_{\text{max}}-2}} P_{n_{\text{max}}}^{\text{direct}}. \quad (13)$$

A similar expression results for the scattering of any directly generated Ly- $n'$  photon into a Ly- $n$  photon,

$$P_{n', n}^{\text{direct-cascade}} = \frac{P_{n', n}}{1 - p_{\text{surv}, n}} P_{n'}^{\text{direct}}. \quad (14)$$

Each cascade generated Ly- $n$  photon in turn serves as a source of further lower order Lyman photons. Considerations similar to the above result in the net cascade-generated collision rate

$$P_n^{\text{cascade}} = \frac{1}{1 - p_{\text{surv}, n}} \sum_{n'=n+1}^{n_{\text{max}}} P_{n', n} P_{n'}, \quad (15)$$

where the total scattering rate of Ly- $n'$  photons is  $P_{n'} = P_{n'}^{\text{direct}} + P_{n'}^{\text{cascade}}$ . The cascade scattering rates may be solved for iteratively starting from higher order to low with  $P_{n_{\text{max}}} = P_{n_{\text{max}}}^{\text{direct}} = P_{n_{\text{max}}}^{\text{inc}} / (1 - p_{\text{surv}, n_{\text{max}}})$ . For Ly $\alpha$  photons ( $n = 2$ ), the same expression may be used except that  $1/(1 - p_{\text{surv}, n})$  must be replaced by  $N_{\text{scat}} = \tau_\alpha$  to account

for the accumulation of Ly $\alpha$  photons as they grow in density once trapped in the IGM, ultimately redshifting away. It is the set of total rates  $P_n$  that drives collisional photon heating and the W-F effect extended to higher Lyman orders.

It will be convenient below to express the scattering rates in terms of the mean photon occupation number of the resonance line photons averaged over the resonance line scattering profile  $\mathcal{N}_{\nu_n} = (c/8\pi)\lambda_n^2 \int_0^\infty d\nu n_\nu \phi_V(a_n, \nu)$ , where  $n_\nu$  is the specific photon number density including the enhancements due to cascades from any higher order Lyman series photon scatterings and rescatterings. The scattering rate per atom in the lower state is then  $P_n = (g_u/g_l)A_{ul}\mathcal{N}_{\nu_n}$ , where  $g_u$  and  $g_l$  are the statistical weights of the upper and lower states, respectively, and  $A_{ul}$  is the spontaneous decay rate for the transition. In terms of the occupation numbers, Eq. (8) and Eq. (15) may be used to express the contributions from direct scatters and subsequent cascades to the photon occupation numbers (for  $n > 2$ ) as

$$\mathcal{N}_{\nu_n}^{\text{direct}} = \mathcal{N}_{\nu_n}^{\text{inc}} \mathcal{S}_n / (1 - p_{\text{surv},n}), \quad (16)$$

and

$$\mathcal{N}_{\nu_n}^{\text{cascade}} = \frac{1}{1 - p_{\text{surv},n}} \sum_{n'=n+1}^{n_{\text{max}}} \frac{A(n', 1; 1, 0)}{A(n, 1; 1, 0)} p_{n',n} \mathcal{N}_{\nu_{n'}}, \quad (17)$$

where  $\mathcal{N}_{\nu_{n'}} = \mathcal{N}_{\nu_{n'}}^{\text{direct}} + \mathcal{N}_{\nu_{n'}}^{\text{cascade}}$  is the total occupation number of Ly- $n'$  photons. For Ly $\alpha$  photons,

$$\mathcal{N}_\alpha^{\text{cascade}} = N_{\text{scat}} \sum_{n=4}^{n_{\text{max}}} \frac{A(n, 1; 1, 0)}{A(2, 1; 1, 0)} p_{n,2} \mathcal{N}_{\nu_n}. \quad (18)$$

The mean photon occupation number for the Ly- $n$  transition will also sometimes be indicated by  $\mathcal{N}_{lu}$  where greater specification of the energy levels involved is required. In particular, for Ly $\alpha$  photons in statistical equilibrium with the gas,  $\mathcal{N}_{si} = \mathcal{N}_{ti} \exp(-T_{st}/T_L)$ , where  $\mathcal{N}_{si}$  and  $\mathcal{N}_{ti}$  describe the Ly $\alpha$  photon occupation numbers corresponding to the hyperfine  $n = 2$  states  $i$  and the hyperfine ground state singlet and triplet states, respectively. For higher levels ( $n > 2$ ),  $\mathcal{N}_{si} = \mathcal{N}_{ti}$  may be taken.

The spontaneous decay rates  $A(n, l; n', l')$  are computed following Condon & Shortley (1970). Excellent agreement is found with the rates published in Wiese et al. (1966). The survival probabilities of Ly- $n$  photons computed agree precisely with those tabulated by Pritchard & Furlanetto (2006), and the Ly $\alpha$  production probabilities  $p_{n,2}$  agree precisely with those tabulated by Hirata (2006) and Pritchard & Furlanetto (2006), who cite the fraction of degraded Ly- $n$  photons that produce Ly $\alpha$  photons, expressed in terms of the values given here by  $p_{n,2}/(1 - p_{\text{surv},2})$ .

Representative photon occupation numbers including rescatterings and cascades are shown in Table 2. The values are normalised by the occupation number of incident Ly- $n$  photons assuming an optically thin IGM. A source with constant  $L_\lambda$  is assumed, as this approximates a starburst spectrum at wavelengths just longward of the Lyman edge (Leitherer et al. 1999). Whilst rescatterings increase the numbers of higher order Ly- $n$  photons by the factor  $1/(1 - p_{\text{surv},n})$  above the incident number, cascades add little more. The exception is for Ly $\alpha$  photons, for which cascades substantially boost the photon density because the Ly $\alpha$  photons become trapped in the IGM, leaving only as they redshift through the resonance line frequency. Approx-

imately one third more Ly $\alpha$  photons are obtained compared with previous findings (Barkana & Loeb 2005; Hirata 2006; Pritchard & Furlanetto 2006; Chuzhoy & Zheng 2007). Instead of Eq. (18), these earlier estimates used the equivalent of  $\mathcal{N}_\alpha^{\text{cascade}} = \sum_{n=4}^{n_{\text{max}}} p_{n,2} (\nu_n/\nu_\alpha)^2 \mathcal{N}_{\nu_n}^{\text{inc}}(0)/(1 - p_{\text{surv},n})$ , where  $\mathcal{N}_{\nu_n}^{\text{inc}}(0)$  is the occupation number of the incident Ly- $n$  photons in an optically thin IGM. For a source at  $z_S = 8$  in a  $T = 10$  K IGM, Eq. (18) gives 29 per cent. more cascade-produced Ly $\alpha$  photons at a proper separation of 1 Mpc from the source, 32 per cent. more at 100 kpc, and 33 per cent. more at 20 kpc.

It is emphasised that radiative transfer effects for Ly $\alpha$  photons involving spatial diffusion, which may enhance the density of Ly $\alpha$  photons near a source (Loeb & Rybicki 1999; Chuzhoy & Zheng 2007; Semelin et al. 2007), or recoils, which may suppress the density near line center and so reduce the scattering rate (Chen & Miralda-Escudé 2004; Higgins & Meiksin 2009) have not been included. It is presumed that the Ly $\alpha$  photons produced in cascades will be subject to the same radiative transfer processes as the directly incident photons, so that the enhancements here reflect the fractional increase due to cascades alone. This is not obviously correct, particularly as the injected photons may arrive within the line core, as opposed to the wings as assumed in most previous studies. The actual degree of enhancement will depend on the relative effects of spatial diffusion, recoil, the local rate of expansion or contraction of the scattering medium, and escape from substructures within the IGM.

### 3 COLLISIONAL HEATING BY LYMAN RESONANCE LINE PHOTONS

When Ly $\alpha$  photons are first incident on cold neutral hydrogen gas, they provide a source of heat resulting from the momentum transferred to the atoms by the scattering photons (Madau et al. 1997). This ‘‘recoil heating’’ persists for only a short period before the radiation field reaches statistical equilibrium with the gas through multiple scatters, and establishes thermal equilibrium with the gas (Field 1959b; Madau et al. 1997; Meiksin 2006). Thereafter at most a residual amount of energy transfer remains in a cosmological setting, scaling like  $\gamma$  as photons redshift through the resonance line frequency (Chen & Miralda-Escudé 2004). For typical IGM conditions at high redshifts, the time to achieve thermal equilibrium is about 1–10 yrs, corresponding to several tens to hundreds of scatters (Meiksin 2006); Ly $\alpha$  photon collisional heating subsequently becomes an inefficient heating mechanism.

By contrast, because higher order Lyman resonance line photons do not survive long enough to establish thermal equilibrium with the scattering medium before degrading into lower energy photons, they may provide a significant source of heating provided their scattering rate is sufficiently high. The analysis for Ly- $n$  photons that rescatter as Ly- $n$  photons is identical to that for Ly $\alpha$  photons. In addition to order-preserving scatterings (Ly- $n$  to Ly- $n$ ), scatterings in which the incident Lyman photon degrades into lower energy photons (eg, Ly $\gamma$  into P $\alpha$ , H $\alpha$  and Ly $\alpha$ ), also provide a source of recoil heating. In this case only the photon produced in the scattering event provides a recoil to the atom,

not the subsequent decays, as may be demonstrated as follows.

The 4-momentum of an incoming atom of rest mass  $m_a$  and quantum state energy  $\epsilon_i$  is  $p_{ai} = [\gamma_i(m_a + \epsilon_i/c^2)\mathbf{v}_i, \gamma_i(m_a c + \epsilon_i/c)]$ . The 4-momentum of the incoming photon which it scatters is  $p_{\gamma i} = (h\nu'/c)(\hat{\mathbf{n}}', 1)$ . After the scattering event, the 4-momenta of the atom and photon are  $p_{af} = [\gamma_f(m_a + \epsilon_f/c^2)\mathbf{v}_f, \gamma_f(m_a c + \epsilon_f/c)]$  and  $p_{\gamma f} = (h\nu/c)(\hat{\mathbf{n}}, 1)$ , for a final atomic quantum state of energy  $\epsilon_f$ . Here,  $\gamma_{i,f} = (1 - v_{i,f}^2/c^2)^{-1/2}$ . To lowest order in  $v/c$ , and neglecting  $\epsilon_i$  and  $\epsilon_f$  relative to the rest mass energy of the atom, the resulting frequency shift between the outgoing and incoming photons becomes

$$\begin{aligned} (\nu - \nu') & \left(1 - \frac{\mathbf{v}_i \cdot \hat{\mathbf{n}}}{c}\right) \\ & \simeq \nu' \frac{\mathbf{v}_i \cdot (\hat{\mathbf{n}} - \hat{\mathbf{n}}')}{c} - \frac{h\nu\nu'}{m_a c^2} (1 - \hat{\mathbf{n}} \cdot \hat{\mathbf{n}}') - \frac{\epsilon_f - \epsilon_i}{h}. \end{aligned} \quad (19)$$

The expression reflects the change in frequency between the incoming and outgoing photons, including the change in the energy state of the atom, the Doppler shift due to the motion of the atom, and the recoil, which depends on the ratio  $h\nu\nu'/m_a c^2$  and corresponds on average to an energy loss from the radiation field. This latter term gives rise to the heating of the IGM.

The frequency of an outgoing photon following the spontaneous decay of the atom after a scattering event may be expressed as the limit of an incoming photon with  $\nu' = 0$ . The frequency of the outgoing photon is then

$$\nu = \frac{\epsilon_i - \epsilon_f}{h(1 - \mathbf{v}_i \cdot \hat{\mathbf{n}}/c)}, \quad (20)$$

which expresses the energy difference of the atom and the Doppler shift due to its motion, without any recoil term. As a consequence, whilst recoil due to the scattering of a photon which degrades upon scattering must be accounted for, no recoils result from any subsequent decays of the atom in the non-relativistic limit.

It is shown in the Appendix that the contribution from scatterings in which the incoming photon is degraded is identical in form to that of a surviving photon: it is only the absorption line profile and the incident and scattered photon energies that enter into the average amount of energy exchanged with the gas. (Any subsequent Ly- $n$  photons produced following scattering events in which the original photon is degraded, of course, will also contribute to the recoil heating term if scattered, at a rate depending on the corresponding absorption line profile.)

The resulting total heating rate due to the scattering of Ly- $n$  photons is

$$\begin{aligned} G_n = P_n n_I \frac{h\nu_n}{m_a c^2} \sum_{n'=1}^{n-1} \frac{A(n, 1; n', 0) + A(n, 1; n', 2)}{A_{n,1}} \\ \times h\nu_{nn'} \left(1 - \frac{T}{\langle T_{nn'} \rangle_H}\right), \end{aligned} \quad (21)$$

for an IGM of temperature  $T$  and a harmonic mean light temperature of

$$\langle T_{nn'} \rangle_H = \frac{\nu_{nn'}}{\nu_n} \frac{\int_0^\infty d\nu n_\nu \varphi_V(a_n, \nu)}{\int_0^\infty d\nu \frac{1}{T_n(\nu)} n_\nu \varphi_V(a_n, \nu)}, \quad (22)$$

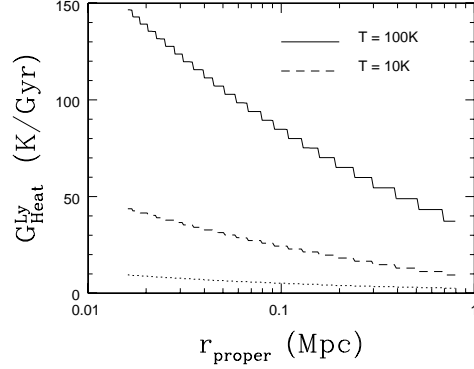


**Figure 2.** Lyman photon collisional heating rate for a source at  $z_S = 8$  and IGM temperatures  $T = 100$  K (solid line) and  $T = 10$  K (dashed line), as a function of proper distance from the source. The heating rate is normalised to a Ly $\alpha$  scattering rate equal to the thermalisation rate  $P_{\text{th}} \simeq 6.8 \times 10^{-12} [(1+z)/9] \text{ s}^{-1}$  required to bring the spin temperature to the kinetic temperature of the IGM through the W-F mechanism. Also shown (dotted line) is the total Ly $\alpha$  scattering rate  $P_\alpha/P_\alpha^{\text{inc}}(0)$  normalised by the scattering rate of the incident Ly $\alpha$  photons not including the contribution from cascades from higher Lyman orders.

where

$$T_n(\nu) = -\frac{h}{k_B} \left( \frac{d \log n_\nu}{d\nu} \right)^{-1} \quad (23)$$

(cf Meiksin (2006)). Here  $\nu_{nn'} = \nu_L(1/n'^2 - 1/n^2)$  (and  $\nu_n = \nu_{n1}$ ), where  $\nu_L$  is the frequency of the Lyman edge.  $A_{n,1}$  is the total decay rate of the  $p$ -state with principal quantum number  $n$ . (Note  $A(n, 1; n', 2)$  is undefined for  $n' < 3$ , and should be regarded as zero.)

The frequency distribution of the photons is determined both by the incident radiation field and the photons produced through rescatterings and cascades. It is convenient to consider the contributions from these secondary photons separately.

Computing the light temperature for the secondary photons requires integrations over the redistribution functions. An estimate may be made most simply for Ly- $n$  photons rescattered into Ly- $n$ . For scatters in the blue wing, the frequency redistribution may be approximated by coherent scattering for which  $R_n(\nu', \nu) \simeq \varphi_V(a_n, \nu) \delta_D(\nu - \nu')$ , where  $\delta_D$  is the Dirac  $\delta$ -function. Eq. (6) then contracts to  $n_\nu^{\text{direct}, n} \simeq n_\nu^{\text{inc}, n} / (1 - p_{\text{surv}, n}) = n_\nu^{\text{inc}, n}(0) \mathcal{S}_n / (1 - p_{\text{surv}, n})$ . For a negligible contribution from the core, the light temperature is then given by

$$\langle T_n^{\text{wing}} \rangle_H \simeq -\frac{h\nu_L}{2k_B} \left(1 - \frac{1}{n^2}\right) \frac{b}{c} x_1$$

$$\begin{aligned} & \times \frac{1 - \exp(-x_1/x_m)}{1 - (1 + x_1/x_m) \exp(-x_1/x_m)} \\ & \simeq -0.0338 \left(1 - \frac{1}{n^2}\right) T^{1/2} x_1 \text{ K}, \end{aligned} \quad (24)$$

where  $x_1 \gg x_m$  has been assumed in the last line. The light temperature is independent of the gas temperature for wing scatters since  $x_1 \sim T^{-1/2}$ . The skewness of the photon number density towards the blue results in a negative light temperature, corresponding to a net transfer of heat to the gas resulting from the Doppler shifting of the photons by the gas. This is in addition to the recoil heating term, and will contribute a comparable amount. Because of the small value of the suppression factor  $\mathcal{S}_n$ , however, the scattering rate will be small, and the heating rate as well.

A larger source of heating will arise from Ly- $n$  photons that first scatter in the core  $x_1 \lesssim x_m$ . In this case, the redistribution function may be approximated in the limit of complete redistribution,  $R_n(\nu', \nu) \simeq \varphi_V(a_n, \nu') \varphi_V(a_n, \nu)$ . Eq. (6) then contracts to  $n_\nu^{\text{direct}, n} \simeq n_\nu^{\text{inc}, n} + n_\nu^{\text{inc}, n}(0) \mathcal{S}_n p_{\text{surv}, n} / (1 - p_{\text{surv}, n})$  for a nearly flat source spectrum  $n_\nu^{\text{inc}, n}(0)$  over the line profile. The light temperature is then

$$\begin{aligned} \langle T_n^{\text{core}} \rangle_{\text{H}} & \simeq \frac{h}{k_{\text{B}}} \frac{\mathcal{S}_n}{1 - p_{\text{surv}, n}} \left[ \int d\nu \exp(-\tau_\nu) \frac{d\varphi_V(a_n, \nu)}{d\nu} \right]^{-1} \\ & \simeq 0.0677 \left(1 - \frac{1}{n^2}\right) T^{1/2} \frac{\mathcal{S}_n}{1 - p_{\text{surv}, n}} \\ & \times \left[ \int dx \exp(-\tau_x) \frac{d\phi_V(a_n, x)}{dx} \right]^{-1} \text{ K}. \end{aligned} \quad (25)$$

Since  $d\varphi_V/d\nu < 0$  blueward of the line centre,  $\langle T_n^{\text{core}} \rangle_{\text{H}} < 0$ , and the radiation field again results in a heating term in addition to the recoil term. The term can be large and even dominate the recoil heating term. Typical temperatures are provided in Table 2. The light temperature scales like  $T^{1/2}$ .

The contribution to the heating from photons produced in cascades depends entirely on integrations over the frequency redistribution functions for the photon products following the scattering of a Ly- $n$  photon which is degraded into lower energy photons (see the Appendix). For example, in the limit of complete redistribution,  $R_{n'n}(\nu', \nu) = \varphi_V(a_{n'}, \nu') \varphi_V(a_n, \nu)$ , the contribution of direct Ly- $n'$  scatters to the number density of Ly- $n$  photons produced through cascades takes the form  $n_\nu^{\text{direct-cascade}, n} \simeq \sum_{n'=n+2}^{n_{\text{max}}} n_\nu^{\text{inc}, n'}(0) (\sigma_{n'}/\sigma_n) \mathcal{S}_{n'} p_{n', n} / (1 - p_{\text{surv}, n})$ . Considerations similar to the above show that the light temperature will be very large in magnitude for a source spectrum  $n_\nu^{\text{inc}, n'}(0)$  nearly flat across the Ly- $n'$  line profile, so that these photons will heat the gas primarily through recoils.

The net heating rate  $G_{\text{Heat}}^{\text{Ly}}$  by higher order Lyman photons is shown in Figure 2 as a function of the distance from a source at  $z_S = 8$  in an IGM with temperatures of  $T = 10$  K and  $T = 100$  K. The steps correspond to the increasing number of Lyman series transitions that contribute to the overall rate through radiative cascades as the source is approached. Almost all the heating results from direct Ly- $n$  photon scatterings; the contribution from cascades is about three orders of magnitude smaller. The heating rates are normalised by the local Ly $\alpha$  photon thermalisation scattering rate  $P_{\text{th}} \simeq 6.8 \times 10^{-12} [(1+z)/9] \text{ s}^{-1}$  (Madau et al. 1997), required to match the scattering rate of CMB photons and so couple the spin temperature to the kinetic temperature of

the neutral hydrogen through the W-F mechanism. (So geometric dilution is not included in the figure: if  $P_\alpha = P_{\text{th}}$  at a particular radius, the heating rate at smaller radii would be larger in proportion to  $1/r^2$ .) When the Ly $\alpha$  intensity is sufficiently strong to initiate the W-F effect, the collisional heating by the scattering of higher order Ly- $n$  photons provides a substantial increase to the temperature of the IGM near a source. An increase in temperature results in a reduction in the Ly- $n$  IGM optical depths (see Figure 1), and a resulting increase in the heating rate. For comparison, also shown in Figure 2 (dotted line) is the radial trend of the enhanced total Ly $\alpha$  scattering rate  $P_\alpha$ , including the effect of cascades from higher orders. The additional contribution due to cascades above the incident Ly $\alpha$  photon rate is found to scale nearly like  $r^{-3/7}$ , although the dependence is somewhat sensitive to the incident source spectrum. It is very insensitive to the IGM temperature.

A fully accurate treatment of the heating rate by higher order Lyman series photons requires solving the radiative transfer equation for both the directly incident photons, with their rescatters, and the photons produced through subsequent radiative cascades. It is expected, however, that the heating rates will be reduced by at most a few per cent., as the photons establish only partial thermal equilibrium with the gas after only a few to several scatters (Meiksin 2006), by which time they will degrade to lower energy photons. Even if the full contribution of photons produced in radiative cascades is excluded, the rate due to the incident higher order Ly- $n$  photons is still substantial.

#### 4 THE WOUTHUYSEN-FIELD EFFECT FOR THE LYMAN SERIES

In this section, the Wouthuysen-Field effect is extended to the scattering of higher order Lyman resonance line photons. Computing the scattering rates at the hyperfine level introduces several complicating factors over Eq. (6) and Eq. (12). First, the redistribution functions defined at the hyperfine level should be used. These are not straightforward, as the ground level is no longer sharp (in particular, the decay from the triplet to singlet states give rise to the 21cm line). Second, a photon emitted at one hyperfine resonance may redshift into a redder hyperfine resonance before rescattering, as  $(\Delta\nu_{\text{hfs}}/\nu_n)c \sim \mathcal{O}(0.1 \text{ km s}^{-1})$ , requiring a travel distance of only 0.1 kpc at  $z = 8$ . Third, for a similar reason the absorption profiles will greatly overlap when the thermal motions of the atoms are included. Fourth, the survival probabilities of individual hyperfine resonance line photons must be used. Fifth, scatters in the wings complicate the averaging over the Voigt profiles since the natural line broadenings of individual hyperfine transitions differ from the total line widths for a Ly- $n$  transition. This latter effect moreover results in a light temperature in the context of the W-F effect that differs from the light temperature of Eq. (22) in the context of photon collisional heating, unlike the case for scattering rates dominated by core scatters (Meiksin 2006).

To make an estimate of the magnitude of the role higher order Ly- $n$  photons play in the W-F mechanism, these effects will be neglected. In particular, it will be assumed that the photons enter the core so that the Voigt profile shapes for the hyperfine transitions are the same as for their par-



ent Ly- $n$  transitions. Since the scattering rates of photons that scatter far in the wings are negligible, this should be a reasonably good approximation to the overall effect. Accordingly, the photon occupation numbers for a given hyperfine transition become the same as for the parent Ly- $n$  transition. The hyperfine scattering rate per atom in the lower state is then  $P_n = (g_u/g_l)A_{ul}\mathcal{N}_{\nu_n}$ , where  $g_u$  and  $g_l$  are the statistical weights of the upper and lower hyperfine structure states, respectively, and  $A_{ul}$  is the spontaneous decay rate for the hyperfine transition.

Because the level populations above the ground state are assumed to be excited exclusively by the scattering of Lyman resonance line photons, in equilibrium the ratio of the occupation number of the excited states to the ground state levels will all be of the order of the photon occupation numbers of the incident Lyman photons or less, depending on the branching ratios from the upper state. The  $2^2S$  state is an exception. Since radiative decays from the  $2^2S$  state to the ground state are forbidden by the selection rules for dipole transitions, this state will fill up until other processes become effective. The dominant mechanism for vacating the state is through two-photon decays. For this state, the occupation number will be larger than the other excited states by a factor on the order of the ratio of the dipole decay rate to the two-photon decay rate, still resulting in occupation numbers much smaller than the ground state levels because of the smallness of the photon occupation number. Accordingly, resonance line scatterings from states above the ground state may be neglected, as these will result in corrections to the state populations quadratic in the photon occupation numbers of the incident radiation field. Denoting the singlet and triplet state occupations by  $n_s$  and  $n_t$ , respectively, and all the hyperfine levels above the ground state by  $n_i$  with  $i = 1$  to  $i = N$  indicating the levels that may be reached by scattering Lyman resonance line photons up to order  $n$ , the radiative cascade equations become

$$\begin{aligned} \frac{dn_s}{dt} &= \sum_{i=1}^N n_i A_{is} - n_s \sum_{i=1}^N g_i \mathcal{N}_{si} A_{is} + P_{ts}^R n_t - P_{st}^R n_s, \\ \frac{dn_t}{dt} &= \sum_{i=1}^N n_i A_{it} - n_t \sum_{i=1}^N \frac{g_i}{3} \mathcal{N}_{ti} A_{it} + P_{st}^R n_s - P_{ts}^R n_t, \end{aligned} \quad (26)$$

and

$$\begin{aligned} \frac{dn_i}{dt} &= g_i A_{is} \mathcal{N}_{si} n_s + \frac{1}{3} g_i A_{it} \mathcal{N}_{ti} n_t + \sum_{j=i+1}^N n_j A_{ji} - \\ & n_i \left( A_{is} + A_{it} + \sum_{j=1}^{i-1} A_{ij} \right), \end{aligned} \quad (27)$$

where  $\mathcal{N}_{si}$  and  $\mathcal{N}_{ti}$  denote the photon occupation number between state  $i$  and the singlet and triplet ground state, respectively,  $A_{ij}$  denotes the electric dipole Einstein  $A$  spontaneous decay rate from hyperfine level  $i$  to hyperfine level  $j$ , and  $g_i = 2F_i + 1$  denotes the degeneracy of hyperfine level  $i$ , where  $F_i = J_i + I$  for total angular momentum  $J_i = L_i + S$ , nuclear spin  $I = \pm 1/2$ , angular momentum  $L_i = l_i$ , where  $l_i$  is the orbital angular momentum of state  $i$ , and electron spin  $S = \pm 1/2$ . The transition rates are computed similarly to the transitions above, but applying the Russell-Saunders multiplet formalism twice to allow for  $J$  and  $I$  coupling to  $F$ . The resulting rates were checked by verifying that applying

the sum rules recovers the fine-structure and full spontaneous decay rates.

It is convenient to label the states by increasing  $n$ , then by increasing  $L$  followed by increasing  $J$  and  $F$ . Since only spontaneous decays from levels  $n$  to levels  $n'$  with  $n' < n$  are considered, this labelling ensures the transitions from states with higher labels to lower will always correspond to transitions from higher energy states to lower. (It is noted that the labelling scheme does not correspond always to increasing energy levels. For example, the  $n^{2S+1}L_J^F = 2^2S_{1/2}^1$  energy level is higher than both the hyperfine levels of  $2^2P_{1/2}$ , Breit & Teller (1940)). Since fine and hyperfine transitions between states with the same principal quantum number are neglected, there is no need to reorder the labelling by energy within these quantum structure levels. If transitions up to  $n = n_{\max}$  are allowed, then the total number of hyperfine states above the  $n = 1$  states is  $N = 2(n_{\max}^2 - 1)$ . Labelling the  $2^2S_{1/2}^0$  state by  $i = 1$  and the  $2^2S_{1/2}^1$  state by  $i = 2$ , the rates  $A_{1s}$  and  $A_{2t}$  are taken to correspond to 2-photon emission at the rate  $A_{2\gamma} = 8.23 \text{ s}^{-1}$  (Spitzer & Greenstein 1951). The corresponding two-photon absorption terms from the ground state singlet and triplet states to the pair of  $2^2S_{1/2}$  hyperfine states are therefore highly negligible and excluded. Eqs. (26) also include radiative excitation and de-excitation between the singlet and triplet hyperfine states, given by the respective rates  $P_{st}^R$  and  $P_{ts}^R$ , to allow for an incident continuum radiation field due to the CMB or nearby radio sources. Similar collisional terms may be added if required.

The excited levels  $n > 1$  will rapidly achieve statistical equilibrium on a timescale of order  $A_{ij}^{-1} \sim \mathcal{O}(10^{-8} \text{ s})$  (except for the  $2^2S_{1/2}$  states, for which the timescale is on the order of 0.1 s). The states may thus be assumed to have reached a steady state, so that Eq. (27) reduces to a matrix equation. It is convenient to renormalise the level occupations by  $\tilde{n}_i = n_i / [n_s \mathcal{N}_L^{\text{inc}}(0)]$ , where  $\mathcal{N}_L^{\text{inc}}(0)$  is the incident photon occupation number just longward of the Lyman edge, and to define the ratio  $r = n_t / n_s$  between the triplet and singlet ground state levels. Denoting the rescaled occupation levels by the vector  $\tilde{\mathbf{n}}$ , the matrix equation for the excited levels becomes

$$\mathbf{M} \cdot \tilde{\mathbf{n}} = \mathbf{y}, \quad (28)$$

where  $\mathbf{M}$  is an upper triangular matrix with diagonal elements  $M_{ii} = A_{is} + A_{it} + \sum_{j=1}^{i-1} A_{ij}$ ,  $M_{ij} = -A_{ji}$  and  $\mathbf{y}$  is an absorption vector with elements  $y_1 = y_2 = 0$  (indicating no 2-photon absorption to states  $i = 1$  and  $i = 2$ ), and  $y_i = g_i A_{is} v_{si} + (g_i/3) A_{it} r v_{ti}$  for  $i > 2$ . Here the notation  $v_{si} = \mathcal{N}_{si} / \mathcal{N}_\alpha^{\text{inc}}(0)$  and  $v_{ti} = \mathcal{N}_{ti} / \mathcal{N}_\alpha^{\text{inc}}(0)$  has been introduced.

Following Field (1958), the value for  $r$  may be determined by casting Eq. (26) in the form

$$\begin{aligned} \frac{dn_s}{dt} &= P_{ts}^{\text{Ly}} n_t - P_{st}^{\text{Ly}} n_s + P_{ts}^R n_t - P_{st}^R n_s, \\ \frac{dn_t}{dt} &= P_{st}^{\text{Ly}} n_s - P_{ts}^{\text{Ly}} n_t + P_{st}^R n_s - P_{ts}^R n_t, \end{aligned} \quad (29)$$

where  $P_{st}^{\text{Ly}}$  and  $P_{ts}^{\text{Ly}}$  are the effective excitation and de-excitation rates of the triplet state by the scattering of Lyman resonance line photons. Defining  $T_{st}$  as the effective temperature corresponding to the 21-cm transition, given by  $hc / (k_B \lambda_{21\text{cm}}) = T_{st} \simeq 0.068 \text{ K}$ , and the 21-cm spontaneous transition rate  $A_{ts} = 2.85 \times 10^{-15} \text{ s}^{-1}$  (Wild 1952), in

equilibrium,  $r = 3 \exp(-T_{st}/T_S)$ , where  $T_S$  is the spin temperature, is given by  $r = (P_{st}^{Ly} + P_{st}^R)/(P_{ts}^{Ly} + P_{ts}^R)$ , where  $P_{st}^R = 3A_{ts}(T_R/T_{st})$  and  $P_{ts}^R = A_{ts}(1 + T_R/T_{st})$ . Here  $T_R$  is the brightness temperature of the incident continuum radiation field at the 21cm transition frequency. In statistical equilibrium without an incident continuum ( $T_R = 0$ ),  $r = 3 \exp(-T_{st}/T_L) = P_{st}^{Ly}/P_{ts}^{Ly}$ , where  $T_L$  is defined as the light temperature, and is identical (to order  $k_B T_{st}/h\nu_\alpha$ ) to the harmonic mean temperature Eq. (22) of the radiation field when the scattering rate is dominated by core scatterers (Meiksin 2006). It relaxes to the kinetic temperature of the gas after a few dozen to a few hundred scatters across the resonance line centre (Field 1959b; Meiksin 2006). Using the definition of  $T_L$  above, the spin temperature may be expressed generally as

$$T_S = T_{st} \left[ \frac{T_{st}}{T_L} + \log \frac{T_{st}(1 + T_R/T_{st})/T_L + y_{Ly}}{T_R \exp(T_{st}/T_L)/T_L + y_{Ly}} \right]^{-1}, \quad (30)$$

where  $y_{Ly} = T_{st} P_{ts}^{Ly}/(T_L A_{ts})$ . (The expression must be modified if electron or atomic collisions are important, here assumed negligible.)

When the light temperature of the Ly $\alpha$  photons has relaxed to the kinetic temperature of the gas, the problem is entirely determined once the triplet de-excitation rate  $P_{ts}^{Ly}$  is specified. For pure Ly $\alpha$  scattering,  $P_{ts}^{Ly} = (4/27)P_\alpha$ , where  $P_\alpha = 3\mathcal{N}_\alpha A_\alpha$  (Field 1958). The higher order generalisation is given by

$$P_{ts}^{Ly} = \sum_{nlJF} \left( \frac{2F+1}{3} \right) \mathcal{N}_{t,(n,l,J,F)} \times A(n,l,J,F; 1, 0, \frac{1}{2}, 1) p_s(n,l,J,F), \quad (31)$$

where  $\mathcal{N}_{t,(n,l,J,F)}$  is the occupation number of photons with frequencies at the hyperfine structure resonance between the ground state triplet state and the state  $(n,l,J,F)$ , and  $p_s(n,l,J,F)$  is the probability that an electron in the hyperfine state  $(n,l,J,F)$  produces a decay to the ground singlet state,

$$p_s(n,l,J,F) = A_{nlJF}^{-1} \sum_{n' < n, l', J', F'} A(n,l,J,F; n', l', J', F') \times p_s(n', l', J', F'). \quad (32)$$

Here,  $A_{nlJF} = \sum_{n' < n, l', J', F'} A(n,l,J,F; n', l', J', F')$  (=  $A_{n,l}$  by the sum rules), is the total decay rate of state  $(n,l,J,F)$ . The probabilities  $p_s$  may be solved for iteratively from Eq. (32), initiated by  $p_s(2, 0, \frac{1}{2}, 0) = 1$ ,  $p_s(2, 0, \frac{1}{2}, 1) = 0$ ,  $p_s(2, 1, \frac{1}{2}, 0) = 0$ ,  $p_s(2, 1, \frac{1}{2}, 1) = 1/3$ ,  $p_s(2, 1, \frac{3}{2}, 1) = 2/3$ , and  $p_s(2, 1, \frac{3}{2}, 2) = 0$ .

The solution to the equations shows the singlet-triplet excitation and triplet-singlet de-excitation rates are boosted only by the increase in the Ly $\alpha$  collision rate  $P_\alpha$  due to the Ly $\alpha$  photons produced in cascades following the scattering of higher order Ly- $n$  photons (Figure 2). The ratio  $P_{ts}^{Ly} = (4/27)P_\alpha$  is found to be accurate to a small fraction of one per cent. even close to a source (down to a proper separation smaller than 20 kpc for a source at  $z_S = 8$ ).

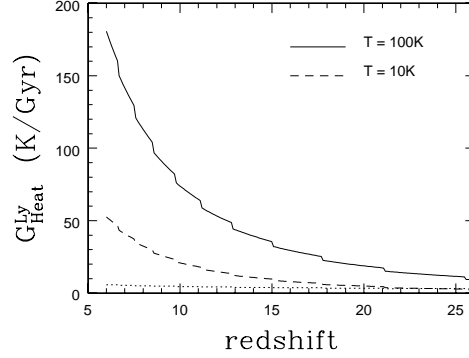


**Figure 3.** Lyman photon collisional heating rate at a distance of 100 kpc from a  $10 M_\odot \text{ yr}^{-1}$  starburst, for source redshifts in the range  $6 < z_S < 26$ . Shown for IGM temperatures of  $T = 100$  K (solid line) and  $T = 10$  K (dashed line). Also shown is the corresponding total Ly $\alpha$  collision rate  $P_\alpha/P_\alpha^{\text{inc}}(0)$ , normalised by the collision rate of the incident photons.

## 5 ASTROPHYSICAL CONSEQUENCES

The redshift  $z_r$  of the reionisation of the IGM is constrained primarily by measurements of intergalactic Ly $\alpha$  absorption in the spectra of high redshift QSOs and by polarisation measurements of the CMB. The spectra of high redshift QSOs constrain  $z_r > 5.7$ , above which the Ly $\alpha$  optical becomes immeasurably large (Fan et al. 2006). The five-year *Wilkinson Microwave Anisotropy Probe* polarisation data yield  $z_r = 11.0 \pm 1.4$  assuming sudden reionisation, with  $2\sigma$  and  $3\sigma$  lower limits of  $z_r > 8.2$  and  $z_r > 6.7$ , respectively (Dunkley et al. 2009). Radio telescope efforts to detect the EoR through its 21cm signature are focussed on appropriate redshift ranges accordingly:  $6.1 < z < 10.8$  (LOFAR),  $z < 17$  (MWA),  $6.1 < z < 27$  (PaST/21CMA) and  $6.1 < z < 13$  (PAPER). Since the impact of higher order Lyman photons on the IGM is sensitive to redshift, the astrophysical consequences are illustrated for a range of redshifts.

### 5.1 Photon collisional heating

The impact Lyman photon collisional heating may have on the temperature of the IGM is illustrated in Figure 3 using a starburst galaxy. A galaxy continuously forming low metallicity ( $Z = 0.05 Z_\odot$ ) stars at the rate  $10 M_\odot \text{ yr}^{-1}$  with masses between  $1 < M < 100 M_\odot$  and a Salpeter IMF will have a steady luminosity at  $\lambda = 915 \text{ \AA}$  of  $L_\nu = 3.8 \times 10^{28} \text{ erg s}^{-1} \text{ Hz}^{-1}$  after about  $10^7$  yrs (Leitherer et al. 1999). This corresponds to a photon occupation number at the Lyman edge of  $\mathcal{N}_\nu \simeq 4.8 \times 10^{-23} r_{\text{Mpc}}^{-2}$ , where the (proper) distance is normalised to 1 Mpc.

The heating rate is found to decline with increasing

source redshift as the IGM becomes increasingly optically thick to Lyman photon scattering, reducing the effective Lyman photon collision rates. A second reduction factor with redshift is the decrease in the number of Lyman orders that may contribute at a fixed proper distance before a photon redshifts into the resonance frequency of the next lower order. Each step in Figure 3 corresponds to a decrease by one order. For comparison, also shown in Figure 3 (dotted line) is the redshift trend of the enhanced total Ly $\alpha$  scattering rate  $P_\alpha/P_\alpha^{\text{inc}}(0)$ , including the contribution from cascades following the scattering of higher order Lyman photons. The rate is normalised by the incident rate excluding the cascade contribution.

Because the optical depth of the IGM diminishes with increasing temperature, the photon collisional heating rate strengthens with increasing temperature, varying as  $G_{\text{Heat}}^{\text{Ly}} \propto T^{1/2}$ . This gives rise to a weak thermal instability that grows quadratically with time. Photon collisional heating may thus produce a substantial increase in the temperature of the IGM surrounding a source and transform an absorption signature against the background CMB into an emission signature (Madau et al. 1997).

## 5.2 W-F effect in the absence of Ly $\alpha$ photons

It was found that the radiative cascades following the scattering of Ly- $n$  photons will enhance the number density of Ly $\alpha$  photons by as much as an order of magnitude near a source. Near a galactic source, however, dust may be present. It is unclear that Ly $\alpha$  photons will be able to survive sufficiently long to build up the photon density required to initiate the W-F effect before being absorbed by dust grains. Observational searches for dust surrounding galaxies suggest dust may be present at least as far out as 100 kpc around low redshift galaxies (Zaritsky 1994; Ménard et al. 2009). If comparable amounts of dust were introduced into the surroundings of galaxies at the time of the EoR following bursts of star formation, then the long total path Ly $\alpha$  photons must travel to migrate from the blue frequencies at which they become trapped in the gas at large distances into the Doppler core, where they become effective scatterers, may exceed the mean free path for dust scattering. The measurement of Ménard et al. (2009) of  $A_V \simeq 2.4 \times 10^{-3} (r_p/100h^{-1} \text{ kpc})^{-0.84}$  at a projected separation of  $r_p$  suggests a mean free path for colliding with dust grains of about  $4 \times 10^5 (r/100h^{-1} \text{ kpc})^{1.74}$  kpc a distance  $r$  from the centre of the galaxy, assuming  $A_\lambda \simeq 1.086 N_d Q_e \sigma_d$  for a column density of  $N_d$  dust grains with cross sections  $\sigma_d$  and an extinction efficiency factor of  $Q_e \simeq 2$  in the visual (Spitzer 1978). For Ly $\alpha$  photons with a mean free path on the order of the distance to which they are able to survive before becoming trapped within the blue wing of an atom, the distance travelled by the photons (of order  $N_{\text{scat}} \simeq 1000$  in the wings times the Ly $\alpha$  mean free path), before diffusing into the resonance line core approaches the mean free path for scattering off a dust grain, which may cause some suppression of the W-F effect. The density of dust around starbursts, however, is likely to be considerably larger than in a normal galaxy, by as much as two orders of magnitude, and may extend to quite large radii (Heckman et al. 2000). In this case the diffuse Ly $\alpha$  photon radiation field required to drive the W-F effect may become substantially suppressed.

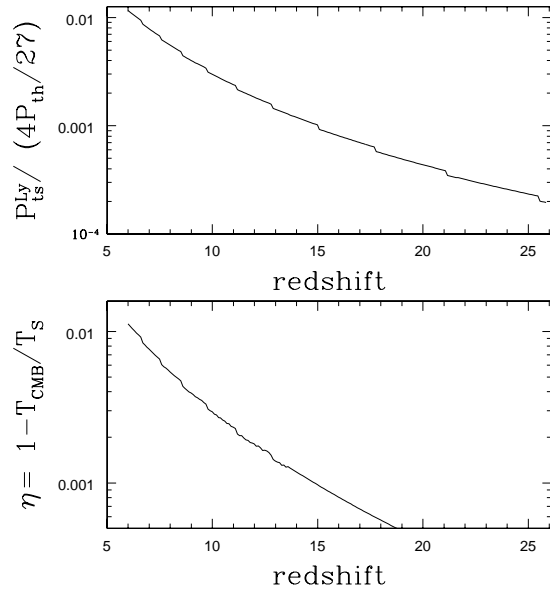


**Figure 4.** (Upper panel) The de-excitation rate of the ground triplet state, normalised by the rate corresponding to the thermalisation scattering rate  $P_{\text{th}}$ , induced by higher order Lyman series photons in the absence of Ly $\alpha$  photons. The rate is shown at a distance of 100 kpc from a  $100 M_\odot \text{ yr}^{-1}$  starburst, for source redshifts in the range  $6 < z_S < 26$ . An IGM temperature  $T = 10$  K is assumed. (Lower panel) The corresponding 21cm radiation efficiency  $\eta$ .

Only the photons that have scattered too few times to have migrated far into the core would contribute.

The loss of the Ly $\alpha$  photons, however, does not mean that the W-F effect will be extinguished. Although far fewer in number, the higher order Lyman series photons will still induce a W-F effect. Because the higher order photons will not achieve thermal equilibrium with the gas, the spin temperature will no longer reflect the kinetic temperature of the gas but rather the net exchange rate between the ground state singlet and triplet levels resulting from collisions by the higher order Lyman photons.

The evolution of the triplet-singlet de-excitation rate at a (proper) distance of 100 kpc from a  $100 M_\odot \text{ yr}^{-1}$  starburst (as above), is shown in Figure 4 (upper panel) for an IGM temperature of  $T = 10$  K. (The results are found to be very insensitive to temperature.) The de-excitation rate is only a fraction of the rate for a total Lyman photon scattering rate matching the thermalisation rate  $P_{\text{th}}$ , but is non-negligible. The light temperature  $T_L$  is found to be high, varying only moderately with redshift, from  $T_L = 170$  K at  $z = 6$  to  $T_L = 200$  K at  $z = 26$ . The spin temperature established, however, must include the scattering of CMB photons. Shown in the lower panel is the resulting 21cm radiation efficiency factor  $\eta = 1 - T_{\text{CMB}}/T_S$ , which controls the strength of the 21cm signal through  $\delta T \simeq \eta T_S (1 - e^{-\tau}) / (1 + z)$ , where  $\delta T$  is the change in the antenna temperature compared with the CMB temperature in a medium with 21cm optical depth  $\tau$  (Madau et al. 1997). Typical efficiency factors of only one per cent. or smaller result, so that a detection would be difficult with the upcom-

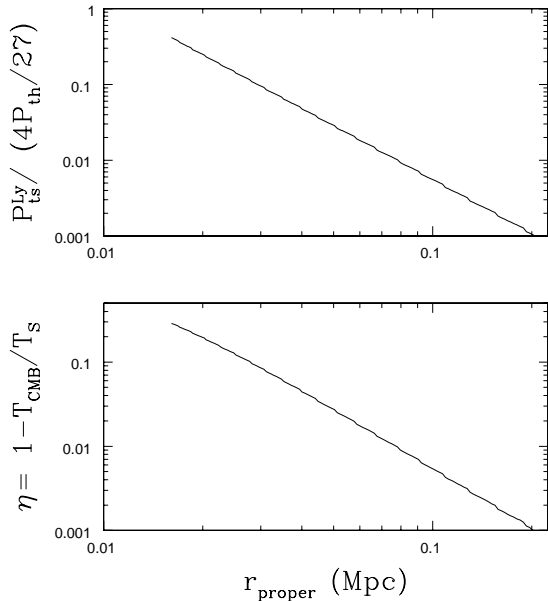


**Figure 5.** (Upper panel) The de-excitation rate of the ground triplet state, normalised by the rate corresponding to the thermalisation scattering rate  $P_{\text{th}}$ , induced by higher order Lyman series photons in the absence of Ly $\alpha$  photons. The rate is shown for a  $100 M_{\odot} \text{ yr}^{-1}$  starburst at  $z_S = 8$ . An IGM temperature  $T = 10$  K is assumed. (Lower panel) The corresponding 21cm radiation efficiency  $\eta$ .

ing telescopes. The efficiency, however, rises at smaller radii, as shown in Figure 5 for the galaxy at  $z_S = 8$ . It is noted the timescale for the Lyman resonance photons to affect the spin temperature will be on the order of  $(P_{ts}^{\text{Ly}})^{-1} \simeq 1$  Myr, so that bursts of shorter duration may not have much effect. A brighter source, however, would increase the signal proportionally. Also, scatters by the residual Ly $\alpha$  photons still outside the resonance line core, not included in the discussion here, will contribute as well, further enhancing the signal.

Although the emphasis in this paper is on the effect of higher order Lyman photons around a single source, a diffuse radiation field will result in regions sufficiently near sources that higher order photons from multiple sources are able to penetrate them before scattering through a lower order Lyman resonance. In this case the collective incident radiation field from the sources is given by

$$J_{\nu} = \frac{1}{4\pi} \int_z^{\infty} dz' \frac{dl_p}{dz'} \frac{(1+z)^3}{(1+z')^3} \langle \epsilon_{\nu'}(z') \exp[-\tau_{\nu}(z, z')] \rangle, \quad (33)$$

(Meiksin 2007), for a source emissivity  $\epsilon_{\nu'}$ , where  $\nu' = \nu(1+z')/(1+z)$ , and  $\tau_{\nu}(z, z')$  is the total optical depth due to all the Lyman resonances (and any other contributing terms) encountered by the photons from gas between the redshifts  $z$  and  $z'$ . The indicated spatial average is over the sources and the IGM optical depth jointly, as these are likely correlated since sources form in overdense regions.

**Table 3.** Scaled emission line photon number emissivities  $\tilde{\epsilon}_{nn'}$  =  $\tilde{n}_n A_{nn'}$  (in units of  $\text{s}^{-1}$ ), for a source at redshift  $z_S = 8$  and a  $T = 10$  K IGM, at (proper) distances from the source of 20 kpc (cols 2–3), 100 kpc (cols 4–5) and 1 Mpc (cols 6–7). The results are shown in pairs of Balmer and Paschen lines with upper principal quantum number  $n$ .

$n$	$\tilde{\epsilon}_{n2}$	$\tilde{\epsilon}_{n3}$	$\tilde{\epsilon}_{n2}$	$\tilde{\epsilon}_{n3}$	$\tilde{\epsilon}_{n2}$	$\tilde{\epsilon}_{n3}$
3	360953.	...	203484.	...	91735.4	...
4	112580.	56787.4	70098.6	33785.3	39451.5	16654.2
5	58433.7	27836.5	39844.4	17841.3	26111.4	10273.5
6	41193.9	18287.5	30835.2	12820.4	23025.4	8617.90
7	32874.8	13850.3	26252.1	10412.6	21148.9	7724.69
8	28240.0	11450.3	23617.6	9085.13	19960.5	7197.96
9	25390.9	10009.5	21964.1	8278.14		
10	23509.6	9077.03	20854.9	7750.76		
11	22200.0	8439.03	20072.8	7387.03		
12	21252.7	7984.15	19501.7	7126.15		
13	20542.8	7647.83	19068.8	6931.77		
14	19996.7	7392.26	18731.9	6782.75		
15	19568.0	7193.75	18464.0	6665.82		
16	19225.1	7036.52	18246.1	6571.86		
17	18946.5	6909.93	18065.2	6494.71		
18	18717.1	6806.52	17912.9	6430.56		
19	18525.8	6720.97				
20	18364.2	6649.25				
21	18227.6	6588.95				
22	18109.9	6537.39				
23	18008.3	6493.12				
24	17919.5	6454.62				
25	17841.7	6421.08				
26	17772.5	6391.43				
27	17710.7	6365.05				
28	17655.4	6341.53				
29	17604.7	6320.09				
30	17558.5	6300.60				
31	17515.8	6282.66				

### 5.3 Cascade radiation emission lines

A consequence of the scattering of Lyman series photons is the generation of a host of intermediate emission lines produced in the cascades following the scattering. The emissivities for these transitions may be computed from the state occupancies given by the solution to Eq. (28).

The scaled Balmer and Paschen photon number emissivities,  $\tilde{\epsilon}_{n2} = \tilde{n}_n A_{n2}$  and  $\tilde{\epsilon}_{n3} = \tilde{n}_n A_{n3}$ , summed over the hyperfine structure lines for a given upper principal quantum number  $n$ , are shown in Table 3 for a source at  $z_S = 8$  at (proper) distances of 20 kpc, 100 kpc and 1 Mpc from the source, for an IGM at temperature  $T = 10$  K. (The emissivities are very insensitive to temperature. The values change by no more than a few per cent. for  $T = 100$  K.) The bolometric emissivities in physical units are then given by  $\epsilon_{ij} = (n_H/4) h\nu_{ij} \mathcal{N}_L^{\text{inc}}(0) \tilde{\epsilon}_{ij}$ , where the factor of 4 takes into account that only 1/4 of the ground state hydrogen atoms are in the hyperfine singlet state (see § 4). The emissivities  $\tilde{\epsilon}_{ij}$  for a source at  $z_S = 20$  are about a factor 5 smaller. The emissivities are found to diminish slowly with distance from the source. The lower order Balmer sequence emissivities scale to better than 8 per cent. accuracy as  $r^{-1/3}$  for H $\alpha$ ,  $r^{-1/4}$  for H $\beta$  and  $r^{-1/5}$  for H $\gamma$ . These scalings apply to

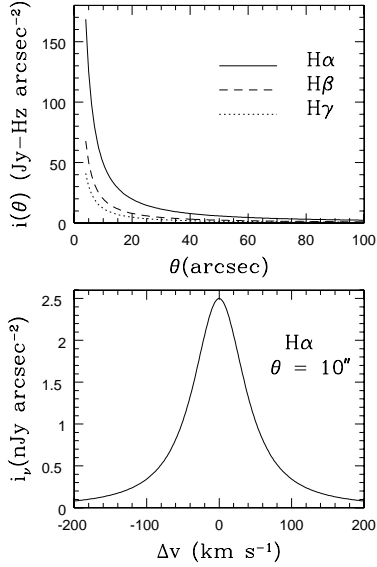


**Figure 6.** Cascade radiation emission line profiles around a  $100M_{\odot}\text{yr}^{-1}$  starburst galaxy at  $z_S = 8$  in an IGM with temperature  $T = 10$  K. (Upper panel) Shown are bolometric  $\text{H}\alpha$ ,  $\text{H}\beta$  and  $\text{H}\gamma$  intensities, corresponding to the respective observed wavelengths of  $5.9\mu\text{m}$ ,  $4.4\mu\text{m}$  and  $3.9\mu\text{m}$ . The integrated fluxes within one arcminute of the source are  $f_{\text{H}\alpha} = 1.6 \times 10^{-18} \text{erg cm}^{-2} \text{s}^{-1}$ ,  $f_{\text{H}\beta} = 8.2 \times 10^{-19} \text{erg cm}^{-2} \text{s}^{-1}$  and  $f_{\text{H}\gamma} = 5.8 \times 10^{-19} \text{erg cm}^{-2} \text{s}^{-1}$ . (Lower panel)  $\text{H}\alpha$  specific intensity at  $\theta = 10$  arcsec.

the Paschen series  $\text{Pa}\alpha$ ,  $\text{Pa}\beta$  and  $\text{Pa}\gamma$  as well. The halo of any given emission line vanishes beyond the horizon of the lowest order  $\text{Ly}-n$  required to generate it.

The bolometric intensity a projected distance  $b$  from a source at redshift  $z_S$  for a bolometric emissivity varying as  $\epsilon_{ij} = \epsilon_{ij}^*(r/r_*)^{-\alpha-2}$  is

$$i_{ij} \simeq \frac{1}{2\pi} \epsilon_{ij}^* r_*^{\alpha+2} (1+z_S)^{-4} \int_0^{\infty} dl (b^2 + l^2)^{-(\alpha+2)/2} \quad (34)$$

$$= \frac{1}{2\pi^{1/2}\alpha} \frac{\Gamma(\frac{1+\alpha}{2})}{\Gamma(\alpha/2)} \epsilon_{ij}^* r_* \left(\frac{r_*}{b}\right)^{1+\alpha} (1+z_S)^{-4}, \quad (35)$$

where the redshift factor has been introduced to convert the bolometric intensity to the value measured at  $z = 0$ . The corresponding specific intensity is

$$i_{\nu} = \frac{1}{4\pi} \frac{c}{H(z)} \frac{\epsilon_{ij}^*}{\nu_{ij}} \frac{1}{(1+z_S)^3} \left[ \left(\frac{b}{r_*}\right)^2 + \left(\frac{\Delta v}{H(z)r_*}\right)^2 \right]^{-(\alpha+2)/2}, \quad (36)$$

where  $\Delta v$  is the velocity difference from line centre. A homogeneous and isotropic medium around the source has been assumed. More realistic line profiles would need to include the structure of the underlying density and velocity fields.

The profiles may be illustrated by the cascade line radiation produced by a  $100M_{\odot}\text{yr}^{-1}$  starburst at  $z_S = 8$  in a  $T = 10$  K IGM. The bolometric intensities for  $\text{H}\alpha$ ,  $\text{H}\beta$  and  $\text{H}\gamma$  are then  $i_{\text{H}\alpha} \simeq 1.1 \times 10^{-20} \theta^{-4/3} \text{erg cm}^{-2} \text{s}^{-1} \text{arcsec}^{-2}$ ,  $i_{\text{H}\beta} \simeq 4.3 \times 10^{-21} \theta^{-5/4} \text{erg cm}^{-2} \text{s}^{-1} \text{arcsec}^{-2}$  and  $i_{\text{H}\gamma} \simeq 2.6 \times 10^{-21} \theta^{-6/5} \text{erg cm}^{-2} \text{s}^{-1} \text{arcsec}^{-2}$ , at an observed angular separation from the source  $\theta$  measured in arcsecs.

The profiles are shown in the upper panel of Figure 6. In the lower panel is shown the specific intensity at  $\theta = 10$  arcsec,  $i_{\nu} \simeq 2.5 \times 10^{-32} \text{erg cm}^{-2} \text{s}^{-1} \text{Hz}^{-1} \text{arcsec}^{-2} [1 + (\Delta v/47 \text{km s}^{-1})^2]^{-7/6}$ .

Although the intensities are small, the integrated fluxes from the emission line halos around the source are appreciable. At  $z_S = 8$ ,  $\text{Ly}\beta$  photons are able to travel as far as 56 Mpc from the source before redshifting into the  $\text{Ly}\alpha$  resonance. This corresponds to an angular distance of  $3.4^{\circ}$ . The total integrated flux is  $f_{\text{H}\alpha}^{\text{tot}} \simeq 5.5 \times 10^{-17} \text{erg cm}^{-2} \text{s}^{-1}$ . Whilst isolating the flux from such an extended halo is likely unfeasible, even within the inner arcminute the total flux is  $f_{\text{H}\alpha}(1') \simeq 1.6 \times 10^{-18} \text{erg cm}^{-2} \text{s}^{-1}$ . Similarly, the fluxes for  $\text{H}\beta$  and  $\text{H}\gamma$  are  $f_{\text{H}\beta}(1') \simeq 8.2 \times 10^{-19} \text{erg cm}^{-2} \text{s}^{-1}$  and  $f_{\text{H}\gamma}(1') \simeq 5.8 \times 10^{-19} \text{erg cm}^{-2} \text{s}^{-1}$ . An observing strategy involving narrow band near infra-red imaging over a wide area would be required to detect the halos. The existence of multiple emission lines has the advantage that it would be possible to correlate the signals in frequency space, with continuum emission from contaminating sources subtracted. For example, defining  $\delta f_{\text{H}\beta} = f_{\text{H}\beta} + f_{\text{cont}} - \langle f_{\text{cont}} \rangle$ , and similarly for  $\text{H}\gamma$ , the correlation of the  $\text{H}\beta$  and  $\text{H}\gamma$  signals is  $\langle \delta f_{\text{H}\beta} \delta f_{\text{H}\gamma} \rangle = \langle f_{\text{H}\beta} f_{\text{H}\gamma} \rangle + [\langle f_{\text{cont}}^2 \rangle - \langle f_{\text{cont}} \rangle^2]$ , so that the signals only need to be detectable above the noise of the continuum across the frequency band of the detector. The emission lines will also give rise to a diffuse sky brightness. At a few such bright sources per square degree, a minimum near infra-red bolometric sky brightness of  $\sim 0.1 \text{mJy sr}^{-1}$  may be expected; the value would be much larger if a much higher density of sources was required to reionise the IGM. Although the detection of individual hyperfine emission lines is unlikely in the near future, it is noted that the state occupancies at the hyperfine structure level are found to scale nearly in proportion to their statistical weights  $2F + 1$ .

It was assumed in § 4 that the optical depths of all levels above the ground  $n = 1$  levels were negligible so that absorptions from them could be ignored. This assumption is now justified. As discussed in § 4, the ratio of the occupancies to the ground state occupancy will be on the order of the photon occupation numbers, and typically much smaller. Only the  $2^2S_{1/2}$  states have large values, of  $10^3 - 10^5$ , because of the smallness of the two-photon decay rate.

The optical depth for transitions between hyperfine states  $i$  and  $j$  is (for absorption from  $i$  to  $j$ ),

$$\begin{aligned} \tau_{ij} &= \lambda_{ij} \sigma_{ij} n_i(z) H(z)^{-1} \\ &\simeq 1549 \frac{g_j}{g_i} \left( \frac{\lambda_{ij}^3 A_{ji}}{\lambda_{\alpha}^3 A_{\alpha}} \right) \tilde{n}_i \mathcal{N}_L^{\text{inc}}(0) (1+z)^{3/2} \end{aligned} \quad (37)$$

where  $\lambda_{ij}^3 A_{ji}$  has been normalised by the value for  $\text{Ly}\alpha$ . Even for the  $2^2S_{1/2}$  hyperfine states ( $n_1$  and  $n_2$  in the notation of this paper), the optical depths will be tiny. Balancing  $n_1 A_{2\gamma} \sim \mathcal{N}_{\alpha}^{\text{inc}}(0) A_{\alpha} n_s$  gives an upper limit  $\tilde{n}_1 \sim \mathcal{O}(A_{\alpha}/A_{2\gamma} \simeq 8 \times 10^7)$ ; in practice the value is more than two orders of magnitude smaller because of the suppression factors  $\mathcal{S}_n$  and reduced cross-sections for  $n > 2$ . Since generally  $\tilde{n}_i < \tilde{n}_1$ , using this generous upper limit for  $\tilde{n}_i$  shows that  $\tau_{ij} < 1$  provided

$$\frac{g_j}{g_i} \left( \frac{\lambda_{ij}^3 A_{ji}}{\lambda_{\alpha}^3 A_{\alpha}} \right) < 8.48 \times 10^{-12} \left[ \mathcal{N}_{\alpha}^{\text{inc}}(0) \right]^{-1} (1+z)^{-3/2}, \quad (38)$$

an equality that is readily met for any relevant transition

and realistic radiation field. As an illustration, for a source at  $z_S = 8$  in a  $T = 10$  K IGM, at a distance of 100 kpc from the source the largest  $n \neq n'$  hyperfine transition optical depth is found for absorption from  $(n, l, J, F) = (2, 0, \frac{1}{2}, 1) \rightarrow (3, 1, \frac{3}{2}, 2)$  with  $\tau \simeq 1.3 \times 10^{10} \mathcal{N}_\alpha^{\text{inc}}(0) \simeq 5 \times 10^{-11}$  for  $\mathcal{N}_\alpha^{\text{inc}}(0) \simeq 3.5 \times 10^{-21}$  corresponding to the thermalisation Ly $\alpha$  scattering rate  $P_{\text{th}}$  at  $z = 8$ .

## 6 CONCLUSIONS

Higher order Lyman series photons from sources at high redshift may have a substantial influence on the 21cm signature from the IGM in the vicinity of the source before the IGM is reionised. Taking into account the diminishing cross section for scattering with increasing order, it is found that Ly- $n$  resonance line photons with  $n \geq 5$  or 6 will first scatter in the resonance line core, where they scatter efficiently. The consequences for the subsequent rate of collisional heating, the intensity of the Wouthuysen-Field effect, and the formation of extended diffuse halos of emission lines produced in radiative cascades are summarised.

Whilst Ly $\alpha$  photons readily establish thermal equilibrium with the IGM, higher order resonance line photons degrade into lower order photons before they are able to do so. Because of the much smaller fraction of higher order Ly- $n$  photons scattered out of a line of sight compared with Ly $\alpha$ , they are able to produce a substantial amount of collisional heating. The heating arises primarily from the blue distortion of the photon density distribution, as only photons blueward of the resonance line frequency are able to survive to large distances without being scattered out of the line of sight. Typical light temperatures for Ly- $n$  photons, where  $n$  is the principal quantum number of the upper state, of  $\langle T_n \rangle_{\text{H}} \approx -0.015T^{1/2}$  K are obtained, where  $T$  is the temperature of the IGM. Resulting collisional heating rates of several tens to hundreds of Kelvin per Gyr are obtained. The heating rate scales as  $T^{1/2}$ , inducing a weak thermal instability in the IGM, with the IGM temperature increasing quadratically with time. One consequence would be that warm regions are heated more rapidly than cooler regions, which would contribute to the patchiness of a 21cm absorption signature against the CMB where the spin temperature is still less than the temperature of the CMB.

Radiative cascades following the scattering of higher order Lyman photons will add substantially to the number density of Ly $\alpha$  photons near a source, enhancing their number by an order of magnitude. The number of Ly $\alpha$  photons produced in cascades is found to be as much as 30 per cent. higher than previous estimates.

Measurements of the dust content in nearby starburst galaxies suggest the W-F effect induced by Ly $\alpha$  photons may be partially suppressed due to the absorption of Ly $\alpha$  photons by dust grains, and possibly even completely eliminated, in the vicinity of starburst galaxies at high redshift during the EoR if comparable amounts of dust were present. It is demonstrated that higher order Lyman series photons will induce a non-negligible W-F effect even in the complete absence of Ly $\alpha$  photons. The 21cm radiation efficiency at distances exceeding 100 kpc from the galaxy would then be one per cent. or smaller except for extremely strong bursts, although the signal is stronger closer to the galaxy. The sig-

nal would still likely be too weak to be discovered around an individual galaxy by first generation 21cm detection experiments, although it may be detectable by a Square Kilometre Array. Future radio detections and upper limits may provide a means of exploiting the suppression to constrain the dust production rates and transport efficiency in high redshift galaxies.

Cascade radiation following the scattering of higher order Lyman photons will produce emission line halos extending over several arcminutes around a source, limited only by the distance to which Lyman photons may travel before redshifting into the resonance frequency of the next lower order. It is shown that the integrated lower order Balmer fluxes within one arcminute surrounding starburst galaxies would be substantial. The detection of the halos would provide a unique means of confirming that candidate reionisation sources are in fact surrounded by an IGM that is still largely neutral.

The effects discussed here are in the context of a homogeneous and expanding universe. Accounting for cosmological structures will modify the results in several ways (Higgins & Meiksin 2009). The local density and velocity fields will affect the mean free paths of the Lyman photons, as will heat input from other possible sources such as Active Galactic Nuclei or Quasi-Stellar Objects. Of particular interest are H II regions surrounding photoionisation sources. The horizons of high order Lyman photons could then be substantially extended as the ionised gas would become optically thin at their resonance frequencies. The collisional heating, W-F effect, and the production of emission line halos would then extend into the neutral gas just beyond the ionisation front. Even with these complications, it is expected that the salient features of the effects discussed here will still be present.

## APPENDIX A: REDISTRIBUTION FUNCTION FOR DEGRADED LYMAN RESONANCE LINE PHOTONS

The redistribution function for an incoming Ly- $n'$  and an outgoing photon other than Ly- $n'$  differs from the normal redistribution function for scattering photons in which the outgoing photon is the same as the ingoing photon (Ly- $n' \rightarrow$  Ly- $n'$ ). The principal difference arises from the re-emission function following absorption. In the case of a preserved Ly- $n'$  photon, the outgoing frequency is the same as the ingoing in the restframe of the atom. In the case of a degraded photon, the outgoing frequency distribution is given by the appropriate Lorentz profile (Weisskopf 1933).

As an example, a scattering event is considered in which a Ly- $n'$  photon is degraded into a final Ly- $n$  photon, with two intermediate transitions (the minimum required to produce a final Lyman photon). The final photon need not be a Ly- $n$  photon; the example only serves to illustrate the computations involved.

Accordingly, four levels are considered in the atom, labelled 0–3, corresponding respectively to the ground state ( $n = 1$ ), the lowest energy excited state, a higher intermediate state, and the  $n'$  energy level. The formalism and notation of Weisskopf (1933) are followed. The absorption

profile for an incoming photon of frequency  $\xi'$  in the frame of the atom is

$$f(\xi') = \frac{1}{\pi} \frac{\delta_3}{(\xi' - \nu_3)^2 + \delta_3^2}, \quad (\text{A1})$$

where the line-centre absorption frequency is  $\nu_3$  and the total decay width of the upper level is  $\delta_3$ . The decay from state 3 to state 2 involves recoil. Because the upper state was excited from a definite energy level (the ground state), the upper energy level is definite. As a consequence, only the uncertainty in the energy level of state 2 will determine the width of the emission profile. Since the atom will decay to the centre of energy level 2 on average, the frequency of the emitted photons will peak at  $\xi = [h\xi' - (\epsilon_2 - \epsilon_0)]/h = \xi' - \nu_2$ , where  $\nu_2 = (\epsilon_2 - \epsilon_0)/h$ . The probability density for emitting a photon of frequency  $\xi$  in the restframe of the atom is then given by

$$p_{3,2}(\xi', \xi) = \frac{1}{\pi} \frac{\gamma_2}{(\xi - \xi' + \nu_2)^2 + \gamma_2^2}, \quad (\text{A2})$$

where  $\gamma_2$  is the decay width of state 2. The redistribution function in the restframe of the atom is given by  $f(\xi')p_{3,2}(\xi', \xi)$ . Note that if the incoming photon is absorbed blueward (redward) of the line-centre, the emitted photon frequency  $\xi$  will also be shifted blueward (redward) of the line centre frequency  $\nu_{23} = (\epsilon_3 - \epsilon_2)/h$ .

For an atom moving at velocity  $\mathbf{v}$  in the laboratory frame, the redistribution function in terms of the incoming and outgoing photon frequencies  $\nu'$  and  $\nu$  in the laboratory frame becomes, allowing for the Doppler shifting of the frequencies to first order in  $v/c$ ,

$$R_v(\nu', \hat{\mathbf{n}}'; \nu, \hat{\mathbf{n}}) = \frac{\delta_3 \gamma_2}{\pi^2} \frac{1}{[\nu' - \nu_3(1 + \mathbf{v} \cdot \hat{\mathbf{n}}'/c)]^2 + \delta_3^2} \times \frac{1}{(\nu - \nu' + \nu_3 \mathbf{v} \cdot \hat{\mathbf{n}}'/c - \nu_{23} \mathbf{v} \cdot \hat{\mathbf{n}}/c + \Delta\nu_{\text{recoil}} + \nu_2)^2 + \gamma_2^2}, \quad (\text{A3})$$

where the recoil term  $\Delta\nu_{\text{recoil}} = (h\nu_3\nu_{23}/m_a c^2)(1 - \hat{\mathbf{n}} \cdot \hat{\mathbf{n}}')$  has been included.

It is convenient to define the dimensionless frequencies

$$x = \frac{\nu - \nu_{23}}{\Delta\nu_D}, \quad x' = \frac{\nu' - \nu_3}{\Delta\nu_D}, \quad \text{with} \quad \Delta\nu_D = \nu_3 \frac{b}{c}, \quad (\text{A4})$$

where the frequencies are normalised by the same Doppler width. The dimensionless decay widths  $a_3 = \gamma_3/\Delta\nu_D$  and  $a_2 = \gamma_2/(\nu_{23}b/c)$  are also introduced, along with the recoil parameter  $\epsilon = h\nu_{23}/m_a b c$  and the dimensionless velocity  $\mathbf{u} = \mathbf{v}/b$ . It is also convenient to introduce the new coordinate system (Hummer 1962)

$$\hat{\mathbf{n}}_1 = \gamma_+ (\hat{\mathbf{n}}' + \hat{\mathbf{n}}), \quad \hat{\mathbf{n}}_2 = \gamma_- (\hat{\mathbf{n}}' - \hat{\mathbf{n}}), \quad \hat{\mathbf{n}}_3 = \hat{\mathbf{n}} \times \hat{\mathbf{n}}', \quad (\text{A5})$$

where  $\gamma_{\pm} = [2(1 \pm \mu)]^{-1/2}$  and  $\mu = \hat{\mathbf{n}} \cdot \hat{\mathbf{n}}'$ . A dimensionless velocity-dependent redistribution function is defined by  $R_u(x', \hat{\mathbf{n}}'; q, \hat{\mathbf{n}}) = (\Delta\nu_D)^2 R_v(\nu', \hat{\mathbf{n}}'; \nu, \hat{\mathbf{n}})$ , where  $q = x - x'$ . It is given by

$$R_u(x', \hat{\mathbf{n}}'; q, \hat{\mathbf{n}}) = \left(\frac{a_3}{\pi}\right) \frac{1}{(x' - \gamma_+^{-1} u_1/2 - \gamma_-^{-1} u_2/2)^2 + a_3^2} \times \left(\frac{\nu_{23} a_2 / \nu_3}{\pi}\right) \left\{ \left[ q + \frac{1}{2} \gamma_+^{-1} u_1 \left(1 - \frac{\nu_{23}}{\nu_3}\right) + \frac{1}{2} \gamma_-^{-1} u_2 \left(1 + \frac{\nu_{23}}{\nu_3}\right) + \epsilon(1 - \mu) \right]^2 \right. \\ \left. + \left(\frac{\nu_{23} a_2}{\nu_3}\right)^2 \right\}^{-1}. \quad (\text{A6})$$

It is convenient to perform the velocity average over a Maxwellian of the redistribution function in Fourier space. The Fourier transform of Eq. (A6) is given by

$$\hat{R}_u(\kappa, \hat{\mathbf{n}}'; \lambda, \hat{\mathbf{n}}) = \int_{-\infty}^{\infty} dx' e^{ikx'} \int_{-\infty}^{\infty} dq e^{i\lambda q} R_u(x', \hat{\mathbf{n}}'; q, \hat{\mathbf{n}}) \\ = \exp\left\{ \frac{1}{2} i \gamma_+^{-1} u_1 \left(\kappa - \frac{\nu_2}{\nu_4} \lambda\right) + \frac{1}{2} i \gamma_-^{-1} u_2 \left[\kappa - \left(1 + \frac{\nu_{23}}{\nu_3}\right) \lambda\right] - i \lambda \epsilon (1 - \mu) - a_3 |\kappa| - \frac{\nu_{23}}{\nu_3} a_2 |\lambda| \right\}. \quad (\text{A7})$$

Averaging over a Maxwellian velocity distribution gives

$$\hat{R}(\kappa, \hat{\mathbf{n}}'; \lambda, \hat{\mathbf{n}}) = \pi^{-3/2} \int d^3 u e^{-u^2} \hat{R}_u(\kappa, \hat{\mathbf{n}}'; \lambda, \hat{\mathbf{n}}) \\ = \exp\left[ -a_3 |\kappa| - \frac{1}{4} \kappa^2 - \frac{\nu_{23}}{\nu_3} a_2 |\lambda| - i \epsilon (1 - \mu) \lambda + \frac{1}{2} \kappa \lambda - \frac{1}{4} \left(1 + \frac{\nu_{23}^2}{\nu_3^2}\right) \lambda^2 - \frac{1}{2} \frac{\nu_{23}}{\nu_3} (\kappa - \lambda) \lambda \mu \right]. \quad (\text{A8})$$

Moments of the dimensionless frequency shift are given by

$$a_n(x, \mu) = \int_{-\infty}^{\infty} dq q^n R(x', \hat{\mathbf{n}}'; q, \hat{\mathbf{n}}). \quad (\text{A9})$$

The Fourier transforms of the moments may be expressed as

$$\hat{a}_n(\kappa, \mu) = \left. \frac{\partial^n}{\partial (i\lambda)^n} R(\kappa, \hat{\mathbf{n}}'; \lambda, \hat{\mathbf{n}}) \right|_{\lambda=0}, \quad (\text{A10})$$

noting that the factor  $q^n$  corresponds to the  $n^{\text{th}}$  derivative with respect to  $i\lambda$  in Fourier space. The transformed moments are readily computed from Eq. (A8). Angle averaging the results and Fourier transforming back to frequency space give for the first three moments,

$$a_0(x) = \phi_V(a_3, x), \\ a_1(x) = \frac{1}{2} \frac{d\phi_V(a_3, x)}{dx} - \epsilon, \\ a_2(x) = \frac{1}{2} \left(1 + \frac{\nu_{23}^2}{\nu_3^2}\right) \phi_V(a_3, x) - \epsilon \left(1 + \frac{1}{3} \frac{\nu_{23}}{\nu_3}\right) \frac{d\phi_V(a_3, x)}{dx} + \frac{1}{4} \left(1 + \frac{1}{3} \frac{\nu_{23}^2}{\nu_3^2}\right) \frac{d^2 \phi_V(a_3, x)}{dx^2}, \quad (\text{A11})$$

where only the first order terms in  $\epsilon$  are retained. The first order moment  $a_1(x)$  is of the same form as for the scattering of Ly- $n$  to Ly- $n$  (Meiksin 2006), and results in the heating rate given by Eq. (21). The Fourier transform of the redis-

tribution function averaged over angle is

$$\begin{aligned} \hat{R}_{3,23}(\kappa, \lambda) &= \frac{\sinh \left[ \frac{1}{2} \frac{\nu_{23}}{\nu_3} \lambda \left( \kappa - \lambda - 2i\epsilon \frac{\nu_3}{\nu_{23}} \right) \right]}{\frac{1}{2} \frac{\nu_{23}}{\nu_3} \lambda \left( \kappa - \lambda - 2i\epsilon \frac{\nu_3}{\nu_{23}} \right)} \\ &\times \exp \left[ -a_3 |\kappa| - \frac{1}{4} \kappa^2 - \frac{\nu_{23}}{\nu_3} a_2 |\lambda| \right. \\ &\left. - i\epsilon \lambda + \frac{1}{2} \kappa \lambda - \frac{1}{4} \left( 1 + \frac{\nu_{23}^2}{\nu_3^2} \right) \lambda^2 \right], \quad (\text{A12}) \end{aligned}$$

where the subscript on  $\hat{R}_{3,23}(\kappa, \lambda)$  indicates the scattering of a photon of frequency  $\nu_3$  to  $\nu_{23}$ .

Similar redistribution functions may be defined for the decay product photons of frequencies  $\nu_{12}$  and  $\nu_1$ , however the analysis become considerably more complicated as transitions between non-sharp levels are involved. Following the discussion of Weisskopf (1933), the frequency distributions may be multiply peaked and correlated with the frequencies of previously emitted photons. For example, for photons absorbed and emitted in the Lorentz wings, the distribution of photons produced in the transition from level 2 to level 1 could have two peaks. In one, the emitted frequency would be correlated with the frequency  $\nu_P$  of the photon emitted in the transition  $3 \rightarrow 2$ , peaking at  $\nu' - \nu_P - \nu_1$ , followed by a transition  $1 \rightarrow 0$  with the photon frequencies peaking at  $\nu_1 = (\epsilon_1 - \epsilon_0)/h$ . A second peak would occur at the frequency  $\nu_{12} = (\epsilon_2 - \epsilon_1)/h$ , with the transition  $1 \rightarrow 0$  producing photons peaking in frequency at the difference between  $\nu_2$  and the frequency of the photon emitted in the  $2 \rightarrow 1$  transition. As the most probable frequency for the final emitted Lyman photons (in this example) is independent of the incoming frequency  $\nu'$ , a good approximation to the redistribution function Ly- $n'$  to Ly- $n$  is  $R_{n',n}(\nu', \nu) = \varphi_V(a_{n'}, \nu') \varphi_V(a_n, \nu)$ .

## REFERENCES

- Bahcall J. N., Ekers R. D., 1969, *ApJ*, 157, 1055  
 Barkana R., Loeb A., 2005, *ApJ*, 626, 1  
 Breit G., Teller E., 1940, *ApJ*, 91, 215  
 Chen X., Miralda-Escudé J., 2004, *ApJ*, 602, 1  
 Chuzhoy L., Zheng Z., 2007, *ApJ*, 670, 912  
 Condon E. U., Shortley G. H., 1970, *The theory of atomic spectra*. (Cambridge: Cambridge University Press)  
 Dijkstra M., Lidz A., Pritchard J. R., Greenhill L. J., Mitchell D. A., Ord S. M., Wayth R. B., 2008, *MNRAS*, 390, 1430  
 Dunkley J., Komatsu E., Nolte M. R., Spergel D. N., Larson D., Hinshaw G., Page L., Bennett C. L., Gold B., Jarosik N., Weiland J. L., Halpern M., Hill R. S., Kogut A., Limon M., Meyer S. S., Tucker G. S., Wollack E., Wright E. L., 2009, *ApJS*, 180, 306  
 Fan X., Carilli C. L., Keating B., 2006, *Ann. Rev. Astron. Astrophys.*, 44, 415  
 Field G. B., 1958, *Proc. I.R.E.*, 46, 240  
 Field G. B., 1959a, *ApJ*, 129, 536  
 Field G. B., 1959b, *ApJ*, 129, 551  
 Furlanetto S. R., Oh S. P., Briggs F. H., 2006, *Phys. Rep.*, 433, 181  
 Furlanetto S. R., Pritchard J. R., 2006, *MNRAS*, 372, 1093  
 Gunn J. E., Peterson B. A., 1965, *ApJ*, 142, 1633  
 Heckman T. M., Lehnert M. D., Strickland D. K., Armus L., 2000, *ApJS*, 129, 493  
 Higgins J., Meiksin A., 2009, *MNRAS*, 393, 949  
 Hirata C. M., 2006, *MNRAS*, 367, 259  
 Hogan C. J., Rees M. J., 1979, *MNRAS*, 188, 791  
 Hummer D. G., 1962, *MNRAS*, 125, 21  
 Leitherer C., Schaerer D., Goldader J. D., González Delgado R. M., Robert C., Kune D. F., de Mello D. F., Devost D., Heckman T. M., 1999, *ApJS*, 123, 3  
 Loeb A., Rybicki G. B., 1999, *ApJ*, 524, 527  
 Madau P., Meiksin A., Rees M. J., 1997, *ApJ*, 475, 429  
 Meiksin A., 2006, *MNRAS*, 370, 2025  
 Meiksin A. A., 2007, *ArXiv e-prints*, 0711.3358  
 Ménard B., Scranton R., Fukugita M., Richards G., 2009, *ArXiv e-prints*, 0902.4240  
 Mihalas D., 1978, *Stellar atmospheres* (2nd edition). (San Francisco: W. H. Freeman and Co.)  
 O'Meara J. M., Burles S., Prochaska J. X., Prochter G. E., Bernstein R. A., Burgess K. M., 2006, *ApJ*, 649, L61  
 Pritchard J. R., Furlanetto S. R., 2006, *MNRAS*, 367, 1057  
 Scott D., Rees M. J., 1990, *MNRAS*, 247, 510  
 Semelin B., Combes F., Baek S., 2007, *A&Ap*, 474, 365  
 Spitzer L., 1978, *Physical processes in the interstellar medium*. (New York, Wiley-Interscience)  
 Spitzer L. J., Greenstein J. L., 1951, *ApJ*, 114, 407  
 Weisskopf V. F. I., 1933, *The Observatory*, 56, 291  
 Wiese W. L., Smith M. W., Glennon B. M., 1966, *NSRDS-NBS 4, Atomic transition probabilities. Vol. I: Hydrogen through Neon. A critical data compilation*. (Washington, D.C.: US Department of Commerce, National Bureau of Standards)  
 Wild J. P., 1952, *ApJ*, 115, 206  
 Wouthuysen S. A., 1952, *AJ*, 57, 31  
 Zaritsky D., 1994, *AJ*, 108, 1619